MASTER'S DISSERTATION

Practical Considerations when Inferring Lightning Current from Electric Field Recordings with a High Noise-Floor

Jarren Hilton Lange

A dissertation submitted to the Faculty of Engineering and the Built Environment, University of the Witwatersrand, in fulfilment of the requirements for the degree of Master of Science in Engineering.

Johannesburg, 2015

Declaration

I declare that this dissertation is my own unaided work. It is being submitted for a Degree of Master of Science to the University of the Witwatersrand, Johannesburg. It has not previously been submitted for any degree or examination to any other university.

Jarren Hilton Lange	Date

Abstract

During a cloud to ground lightning event a charge centre within the storm cloud is discharged. The discharge of a charge centre within the cloud leads to a change in the electric field radiated by the charge centre. It is theoretically possible to infer the lightning current from the derivative of the electric field. It is only possible to infer the lightning current from the electric field data where the noise is comparatively much smaller than the electric field data. The changing electric fields for a lightning event that occurred on the 3^{rd} January 2015 13:15:13 were recorded by a flat plate electric field sensor with a passive integrator. The oscilloscope used to capture the electric field data has a relatively large measurement noise and a low resolution. A low pass digital filter was applied to the recorded electric field data to reduce the effects from the high frequency noise. The lightning strokes were recorded by the South African Lightning Detection Network. The Lightning Detection Network data is used to obtain the distance of the lightning event from the sensor, to scale the inferred lightning current. The Lightning Detection Network also provides a lightning peak current measurement to compare to the peak current inferred from the electric field data. The lightning stroke current was inferred from the electric field recording for various bandwidths of the low pass filter. Inconsistent changes to the inferred lightning stroke current as the filter bandwidth is changed shows that the frequency components for each stroke differs. The peak stroke current was not constant for any filter bandwidth range implying that the measurement noise is relatively too large. The case study presented demonstrates that with a relatively large noise magnitude (3 to 4 discrete steps of the digital recording) compared to the electric field signal (21 discrete steps) it is difficult to accurately infer the lightning current from the electric fields recorded.

Acknowledgements

The author would like to thank both Prof. Ken Nixon and Mr. Hugh Hunt for their assistance. Gratitude is given to Eskom for their support of the High Voltage Engineering Research Group at Wits University through TESP. The author would also like to express gratitude to the Department of Trade and Industry (DTI) for THRIP funding and to thank the National Research Foundation (NRF) for direct funding of the research group. The financial assistance of the National Research Foundation (NRF) towards this research is hereby acknowledged. Opinions expressed and conclusions arrived at, are those of the author and are not necessarily to be attributed to the NRF. Lastly, to my parents for permission to turn the house and my room into my own personal laboratory along with their undying support and motivation.

Contents

List of Figures

List of Tables

List of Symbols

Symbol	Description	Units
$\vec{E}$	Electric field observed	Volt/Metre [V/m]
A	Surface Area	Square Metre [m^2]
q	Charge	Coulomb [C]
H_c	Height of Charge above ground	Metre [m]
ϵ	Absolute Electromagnetic Permittivity	Farad/Metre [F/m]
d	Distance from lightning stroke	Metres [m]
E_z	Electric field observed along the z-axis	Volt/Metre [V/m]
h	Height of tip of stepped leader above ground	Metre [m]
ρ	Charge density of a line of charge	Coulomb/Metre [C/m]
D	Electric Displacement	Coulomb per Square Metre [C/m^2]
Z	Electric Impedance	Ohm [Ω]
C	Electric Capacitance	Farad [F]
L	Electric Inductances	Henry [H]
R	Electric Resistance	Ohm [Ω]
f	Frequency	Hertz [Hz]
ω	Angular Frequency	Radian/Second [rad/s]
V	Voltage	Volt [V]
i	Current	Amp [A]

Chapter 1

Introduction

In South Africa alone there are at least 260 fatalities attributed to lightning each year. Even more people are injured from lightning each year. Non-lethal injuries range from nerve damage, chronic pain and psychological conditions. The cause of many of these injuries can be attributed to a lack of knowledge leading to false beliefs and ideas and hence the wrong actions to avoid lightning injury [1–3].

Lightning can be a cause of forest fires and damage to infrastructure and electrical equipment. Electrical equipment has been damaged due to both direct or indirect (induced) effects. The national electrical energy supplier to South Africa, Eskom, reports that 26% of all transmission line failures can be attributed to lightning [4]. As society relies more on electrical equipment to conduct day-to-day activities the development of better protection mechanisms which are incorporated into the design process of electrical systems is of greater importance. The design and testing of these protection measures is dependant on accurate knowledge of the lightning event.

Therefore the study and research of lightning is extremely important to minimize the damage it causes. Electric field observations is one measurement tool that can help improve our knowledge of lightning in order to develop better protection mechanisms from lightning. Specifically the radiated electromagnetic fields from a lightning event can be used to infer the location of the lightning stroke, the lightning current and the type and polarity of the

stroke. Since the properties of lightning differs between locations, understanding and characterising the lightning in a specific location can assist in improving the design of protection mechanisms. Having information about the lightning current and its waveform, for instance, allows us to simulate and reproduce the lightning current safely in a laboratory. This allows for the better design and testing of electrical equipment protection against such lightning currents.

Fast electric field measurements for naturally triggered lightning strokes have been conducted at lower altitude locations, such as USA (Florida, Camp Blanding, approx. 70 m), Brazil (Säo José dos Campos, approx. 660 m), India (Pune, approx. 560 m) and Austria (Salzburg, approx 1300 m) [5–8].

This document embodies the results from work performed during the year of 2014/2015 in an attempt to establish an electric field measurement system in Johannesburg, South Africa. This can be achieved by establishing a measurement system for exploring the fast electromagnetic fields emitted during cloud-to-ground lightning. It is theoretically possible to infer the lightning event current from the radiated electric fields. However the electric field recordings will have unwanted artefacts, such as measurement noise inherent in the digital conversion process.

This document explores the practical problems inherent when inferring the lightning stroke current from noisy and low resolution electric field data. This is achieved by recording a low signal voltage from the electric field sensor with equipment with known noise performance issues.

1.1 Approach Taken

The lightning electric field current can theoretically be inferred from the electric fields radiated during a lightning event. Noise in the measurement of these electric fields will result in errors in the measured lightning currents. The electric fields radiated by a lightning event is captured in an experiment to investigate the effects of the measurement noise.

1.1.1 Problem Statement

Understanding the lightning discharge process is vital in trying to understand how lightning events damages electrical equipment. The lightning event current is useful in improving the accuracy of the model. Direct measurement of the lightning current is difficult. Inferring the lightning current from the lightning event electric fields is an alternative technique. Due to the relatively low signal magnitude of the electric field sensor measurement noise needs to be considered in the design of an electric field sensor.

In order to infer the lightning current from the electric fields the electric field derivative needs to be determined. The electric field recording will include measurement noise. The low signal voltage of the electric field sensor with the relatively large magnitude of the measurement noise means inferring the lightning current accurately is problematic.

It is therefore desirable to investigate the effect of the measurement noise on inferring the lightning current from electric field recordings with a significant noise floor. In order to achieve this the electric fields for lightning events will be recorded. The electric fields will be recorded with an instrument with a low resolution and relatively high noise magnitude. A filter will be applied to the recorded electric fields to reduce the noise. The filter's bandwidth will be adjusted to evaluate if there is an ideal filter bandwidth that will reduce the noise, without affecting the lightning current information.

1.1.2 Proposed Methodology

The proposed methodology is to use a flat plate electric field sensor to measure the electric fields from a cloud to ground lightning event. The electric fields will be recorded by measurement equipment with a poor resolution and relatively high measurement noise. A low pass filter will be applied to the electric field recordings to increase the effective resolution and to decrease the effect of the noise. The lightning current will then be inferred from the recorded electric fields for various filter bandwidths. The inferred lightning event current will be compared to the lightning current recorded by the South African Lightning Detection Network.

1.2 Chapter Overview

This document has been divided into several chapters.

Chapter 2 includes a literature review and discusses current knowledge about lightning and its associated electric fields. This includes how lightning occurs and how the change in charge of a lightning event results in a change in the electric fields. The design of the electric field sensor is presented. An equation to determine the lightning current from the electric field changes is derived using the theoretical electric field models. Finally the possible effect of noise on the lightning current results is explained.

Chapter 3 details the methodology and process applied to obtain the recordings. The technique used to obtain the electric fields is presented. The methodology used to analyse the effects of the noise on the lightning current inferred from the lightning event is detailed. Equipment with a large noise magnitude is used.

Chapter 4 applies the methodology presented in Chapter 3 to the electric fields recorded of a lightning event that occurred 4.28 km from the sensor. The lightning current is inferred from the electric fields for various filter frequencies. The peak current from each filter cut-off frequency is compared. The results from the analysis is discussed. Recommendations are made that may reduce the effect of the noise.

Chapter 5 concludes the document with a summary of the information presented in this document.

Chapter 2

Background

The background theory behind the experiment detailed in this dissertation needs to be understood in order to analyse the results of the experiment. Current knowledge of the lightning mechanism needs to be understood in order to create a model to explain the radiated electric fields. The means of measuring the electric fields is explained in the design of the flat plate electric field sensor. Post-processing is applied to the recorded signals to remove non-ideal effects inherent in the measurement setup. A low-pass filter reduces the recorded noise and increases the effective resolution of the recorded signal. The lightning event instantaneous current can be inferred from the recorded lightning event electric fields using the electric field model. The effect of noise in this process is theoretically analysed in order to explain the expected results.

2.1 Overview

Current knowledge on the lightning discharge process models the lightning cloud as a tri-pole charge arrangement. These charge centres create an electric field between the cloud and the ground. When a lightning discharge occurs, a charge centre is discharged. The decrease of the charge within the charge centre results in a decrease in the electric fields between the cloud to the ground. This changing electric field creates a proportional change in charge on a sensor plate. This change in charge is integrated by a passive in-

tegrator which has a non-ideal resistive decay. The resistive decay and noise within the recorded signal is compensated for with post-processing. From the resultant electric field recording it is possible to infer the lightning event instantaneous current. However the noise in the recorded signal will affect the results of the the lightning current inference process.

2.2 The Lightning Discharge Process

In South Africa, negative cloud-to-ground lightning accounts for 90.3 % of all cloud to ground lightning [9]. This negative cloud to ground lightning discharge process can be broken up into four distinctive processes: the build-up of charge, the stepped leader, attachment and the subsequent strokes.

2.2.1 Charge Accumulation

The cumulonimbus cloud, commonly known as the thundercloud is the charge source for most of the lightning on Earth. The charge structures within the cumulonimbus clouds are generally modelled as a vertically stacked tri-pole structure, with positive charges on top, negative in the middle and a smaller positive charge on the bottom (Figure 2.1(a)). The top two charges have a charge of about 40 C, with the bottom charge being an order of magnitude less. The charge separation mechanisms involve the electrification of atmospheric water (hydrometeors) and a the separation of these charged hydrometeors by their polarity (such as the convection mechanism [10]) [11–13].

2.2.2 Stepped Leader

A stroke is initiated in the region of a negative charge centre where the electric field intensity approaches the ionization field intensity ($3kV/mm$ for atmospheric air or $1kV/mm$ in the presence of hydrometeors). Many of these strokes will be between the various charge centres, called inter-cloud lightning. However some of these strokes may result in the movement of charge through ionized channels, called stepped leaders towards the ground. After exiting the visible cloud, the cloud to ground leader typically displays various branches (Figure 2.1(b)). As the stepped leaders approach the ground,

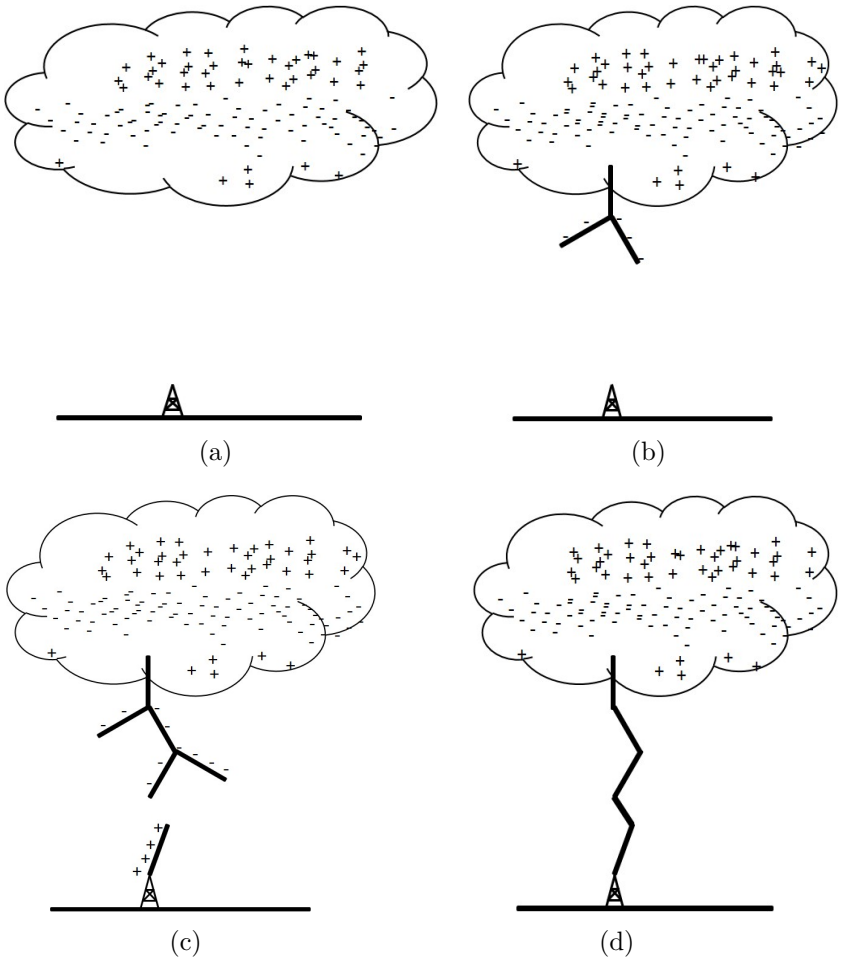

Figure 2.1: Initial formation of the natural cloud-to-ground lightning stroke. When the charge within the cloud reaches a critical level 2.1(a), a local breakdown occurs, leading to the formation of a descending negative stepped leader 2.1(b). As the negative stepped leader approaches the ground the electric fields near the ground increase, resulting in an upward positive leader 2.1(c). When the two leaders meet they attach, leaving a conductive channel for further strokes 2.1(d).

the electric field between the stepped leaders and the ground increases. This increase in the electric field between the stepped leader and earth can cause point discharges from earth objects (such as trees and tall buildings). If the charge concentration at an earth object is high enough, an upwards positive streamer will be initiated (Figure 2.1(c)). The field between the downward leader and the ground is often enhanced due to the presence on protruding objects on the ground [11].

2.2.3 Attachment and Return Strokes

When a positive upward leader meets the negative downward leader there is a large potential difference in the order of several mega-volts [14]. In transmission line model terms, this attachment point can be modelled as a short circuit, with the cloud being an open circuit. This creates an upwards propagating wave, known as a return stroke, which serves to neutralize the charge of the stepped leader. The return stroke is responsible for the visual and auditory phenomena associated with lightning as well as damage and injury. This stepped leader and return stroke sequence is referred to as a leader/return stroke sequence. This leaves a channel of ionized air, through which any resultant charge within the cloud will move through the cloud, through cloud-to-cloud processes, until a subsequent stroke will travel to the ground (Figure 2.1(d)). There are typically 3 to 5 subsequent strokes in a lightning event [12, 14, 15].

The current waveforms from these return strokes has been measured with resistive shunts and current transformers for lightning attaching to towers. This is problematic as the tower itself must be instrumented in order to attach the measurement equipment. The same measurements may be obtained from the electric field recordings which requires no modification to the existing towers [8].

2.3 Electric Field Model

The models for the electric fields radiated by lightning have been analysed previously by Vladislav Mazur and Lothar H. Ruhnke [16]. In their research, the effects of both the charge centre and the lightning stroke are considered

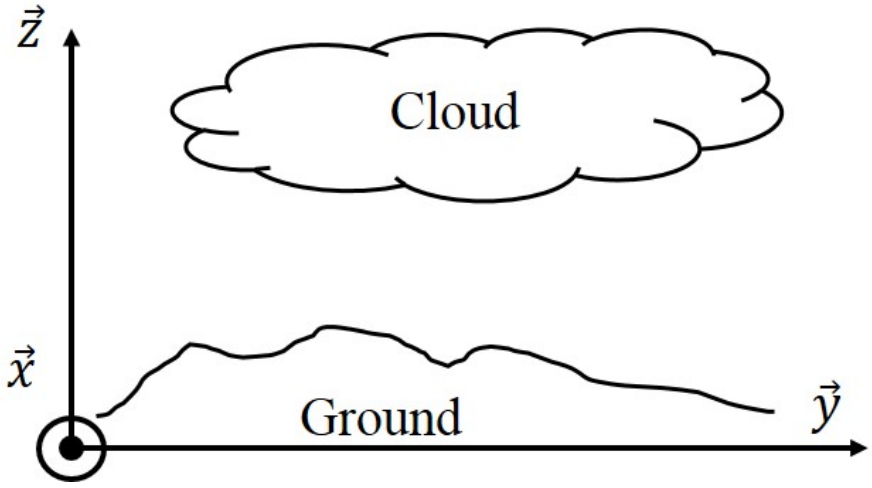

Figure 2.2: Placement of the standard three dimensional Cartesian co-ordinates $(\vec{x}, \vec{y}, \vec{z})$ with respect to the clouds and ground.

together in a Line Charge Model. While this model effectively models the overall electric field, it is difficult to extract information from the electric field if both cases are considered at once. However if the lightning event is far enough from the observer, the electric fields observed are going to be largely determined by the net electric field from the charge centres in the clouds and the ground [16]. This theoretical field model will be applied to the electric field waveforms recorded.

For the model derived below the Cartesian co-ordinates demonstrated in Figure 2.2 are used.

The established lightning model can be simplified to the electric field model, shown in Figure 2.3 [14]. It is assumed that the lightning channel is a vertical line from the attachment point, to the charge centre. The primary electric field change is due to the discharge of the charged particles to ground through the lightning stroke [16]. This is modelled by treating the charge centre being discharged as a single charge centre some distance H_c above a conducting plane. In the model, shown in Figure 2.3, d represents the distance of the observer from the stroke. The mirror-reflect technique is used to create the model presented in Figure 2.3 [17, 18]. In this case the

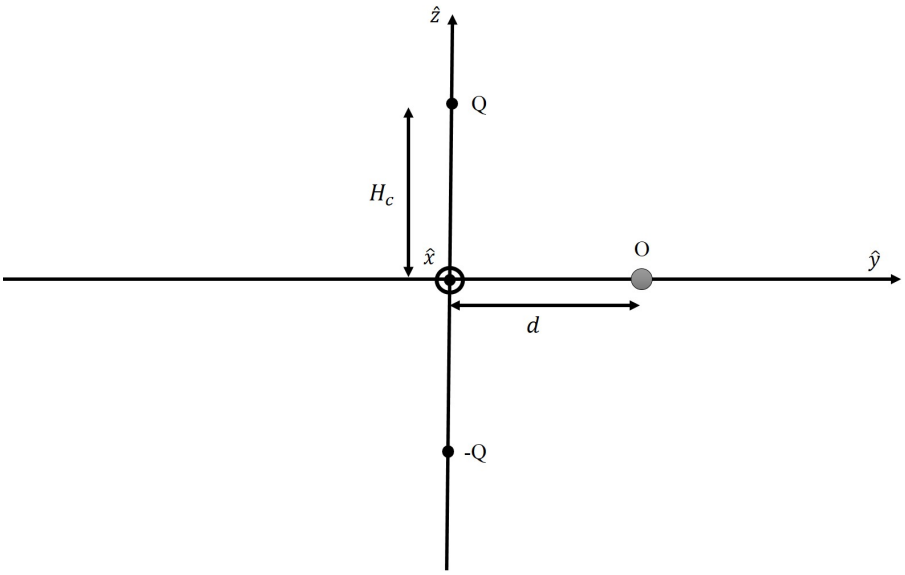

Figure 2.3: Model to analyse electric fields during a lightning event.

charge centre in the cloud is simplified to be a point charge, Q, with charge magnitude, q, at a height of H_c above the ground. With the mirror-reflect technique a charge equidistant from the charge source with charge $-Q$ is created. The model can be analysed as a simple dipole model. In this case the electric field at the observer point O can be explained by Gauss's Law resulting in Equation 2.1 [19].

$$\oint_s \vec{E} \cdot d\vec{A} = -\frac{q\,(2H_c)}{4\pi\epsilon_0} \frac{1}{[d^2 + H_c^2]^{\frac{3}{2}}} \vec{z} \cdot \vec{A} \tag{2.1}$$

If the surface of interest A lies perpendicular to the $\vec{z}$ axis, then the dot product $\vec{z} \cdot \vec{A} = A$. Further if the distances from the charge (both H_c and d) are sufficiently larger than the area of interest, then the electric field over the area can be considered uniform over the area in question. Since d and H_c are typically in the range of a few kilometres, and the sensor diameter is $0.444\ m$, the field over the sensor plate is assumed to be uniform, hence the equation is simplified to the equation to that presented in Equation 2.2.

$$E_z = -\frac{qH_c}{4\pi\epsilon_0}\frac{1}{[d^2 + H_c^2]^{\frac{3}{2}}} \tag{2.2}$$

It is assumed that during a lightning stroke, only the charge concentration vertically above the attachment point is discharged. Thus a lightning stroke results in a single charge centre being depleted. This results in a change in the net electric field change between the cloud and ground. The sensor used is only able to detect changes in the electric field and cannot detect the slower components, DC to 100 Hz (shown in Section 2.4). Therefore the change in the electric field can be determined from the change in charge (Δq)

$$\Delta E_z = -\Delta q\frac{H_c}{4\pi\epsilon_0}\frac{1}{[d^2 + H_c^2]^{\frac{3}{2}}} \tag{2.3}$$

Equation 2.3 corresponds with existing work and research [10, 20, 21]. This model only accounts for the changes to the charge centre affected by a lightning stroke neglecting the effects of the line charge. If the change in the charge centre is known the changes to the electric field can be inferred. It is this electric field change which will be measured by the electric field sensor.

Note the negative sign implies that a positive electric field derivative is indicative of a decrease in the negative charge centre referred to as a negative lightning stroke.

2.4 Electric Field Measurements

The measurement of the vertical component of the electric field $\vec{E_z}$ and its derivative $d\vec{E_z}/dt$ is made possible by the flat plate antenna. The field, $\vec{E_z}$, is the electric field between the cloud and the ground. This electric field is normal to the surface of the earth, as shown in Section 2.3. The horizontal component is normally neglected as the boundary conditions for a perfectly conducting ground state that the electric field component tangential to the earth is zero. The vertical electric field component is the focus of these measurements.

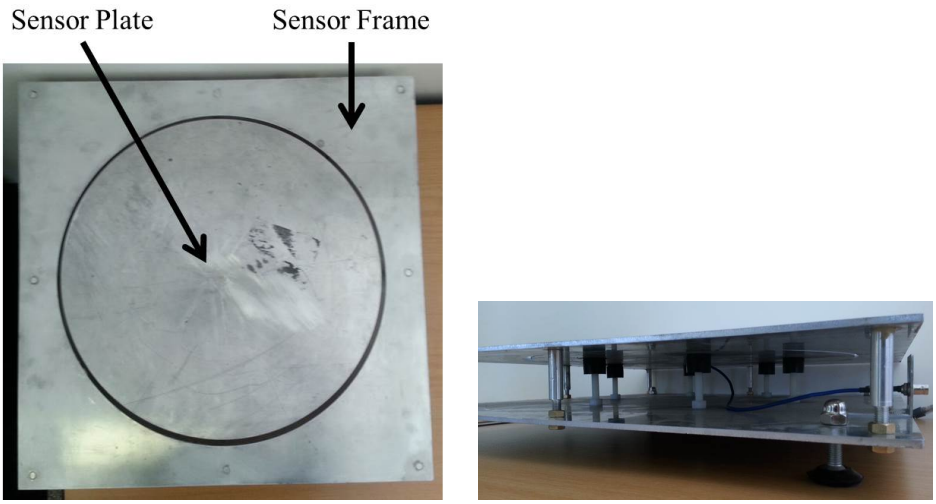

(a) (b)

Figure 2.4: Top view (a) and side view (b) of flat plate electric field sensor used

2.4.1 Flat Plate Electric Field Sensor Construction

The flat plate sensor used in this paper is shown in Figure 2.4. The design of the flat plate sensor follows that presented by Jerauld [12]. The sensor contains a 0.44 m diameter aluminium disc, called the sensor plate, held flush with the top of the sensor frame, separated by a 5 mm annular gap. The frame of the sensor, is a square 0.54 m in length. The frame of the sensor is earthed via the coaxial cable, while the sensor plate is connected to the signal line of a BNC connector. The sensor plate is held isolated from the sensor frame with nylon bolts that are topped with plastic caps, used to stop water from creating a conductive path between the plate and the frame of the sensor along the nylon bolts. The aluminium of the sensor is 4 mm thick, to help the sensor resist damage from hail. The top of the sensor was made as flat and free from protrusions as possible that may lead to electric field concentrations that would distort the results.

2.4.2 Norton Equivalent

The Norton equivalent model for a flat plate antenna can be determined by considering the boundary on an ideally conductive ($\sigma = \infty$) surface.

$$\vec{D} \cdot \hat{n} = \rho_s \tag{2.4}$$

Here the $\vec{D}$ quantity is the electric displacement vector at the surface of the conductor, ρ_s is the surface charge density and $\hat{n}$ is the unit vector perpendicular to the surface. Hence $\vec{D} \cdot \hat{n} = D_n$ is the electric displacement which is normal to the surface. If the normal surface is parallel to the ground (sensor plate parallel with the ground), then the perpendicular coordinate can be equated to that of the z-axis in the Cartesian coordinate system. Therefore Equation 2.4 becomes:

$$\vec{D} \cdot \hat{n} = D_n = D_z = \rho_s \tag{2.5}$$

If the surface is assumed to be an ideal conductor the electric displacement within the conductor and the tangential component of the electric displacement along the conductor are considered zero. Since the medium above the plate is air, which is assumed to be linear, isotropic, homogeneous and non-conductive, the following relationship holds.

$$D_z = \epsilon E_z \tag{2.6}$$

Considering Equations 2.5 and 2.6 and since the permittivity of air is very similar to that of free space ($\epsilon_0 = 8.854187817\ldots \times 10^{-}12$) the equation for ρ_s can be written [17].

$$\rho_s = \epsilon_0 E_z \tag{2.7}$$

The boundary conditions state that if the component of the electric field normal to the surface is uniform over the surface of the plate then the charge density of the plate is uniform. If the smallest waveform of the incident electric field E_z is much larger than the plate, then the charge density of the

plate can be considered uniform. The total charge density is calculated by multiplying the charge density by the surface's area. For a circular plate the electric field is considered uniform if the diameter of the plate is smaller than one-sixteenth of the smallest wavelength. If the largest frequency of E_z is assumed to be less than 30 MHz then the smallest wavelength is 10 metres, one sixteenth of which is 0.625 m. Therefore if the charge density on the plate is uniform, since the maximum frequency of the field is 30 MHz, the total charge on the sensor plate is

$$Q_{plate} = \epsilon_0 A_{plate} E_z \tag{2.8}$$

Electric current is defined as the time derivative of the electric charge, therefore the Norton equivalent short-circuit current for the sensor plate can be expressed

$$i(t) = \frac{d}{dt} Q_{plate}(t) = \frac{d}{dt} \left[\epsilon_0 A_{plate} E_z(t)\right] = \epsilon_0 A_{plate} \frac{dE_z(t)}{dt} \tag{2.9}$$

Hence the flat plate antenna can be viewed as a current source whose magnitude is proportional to the time derivative of the normal or z component of the electric field. This relationship can be taken into the frequency domain by using the Laplace Transform. The Laplace transform $X(s)$, of a time domain signal $x(t)$ is defined by Equation 2.10.

$$\mathcal{L}\left\{x(t)\right\} = X(s) = \int_{t=-\infty}^{\infty} x(t) e^{-st} dt \tag{2.10}$$

By applying the Laplace transform to the equation for the plate current (Equation 2.9) the Norton equivalent in the Laplace domain becomes

$$I(s) = \epsilon_0 A_{plate} s E_z(s) \tag{2.11}$$

Where $E_z(s)$ and $I(s)$ are the Laplace transforms of the electric field $E_z(t)$ and sensor current $i(t)$ respectively.

The Norton equivalent circuit is then completed by an analysis of the impedances that are loading the Norton current source. These are the source

impedance, Z_s , and the load impedance, Z_l. The source impedance, Z_s is the impedance of the source itself where the load impedance, Z_l is the impedance of the load attached to the sensor. These impedances can be resistive, capacitive, inductive or a combination of the three.

If the output of interest is taken to be the voltage across the load impedance ($v_{out}(t) \Leftrightarrow V_{out}(s)$), then the expression for the output voltage in the frequency domain is

$$V_{out}(s) = I(s)Z_{total} = I(s)\left(Z_s \parallel Z_l\right) = s\epsilon_0 A_{plate} E_z(s)\left(\frac{Z_s Z_l}{Z_s + Z_l}\right) \qquad (2.12)$$

The source impedance is largely determined by the capacitance of the antennae itself, C_{ant} [22]. In which case the source impedance is described by Equation 2.13.

$$Z_s = \frac{1}{sC_{ant}} \qquad (2.13)$$

The capacitance of the flat plate antenna (C_{ant}) used was measured to be 100 pF. Any inductance and resistance of the antenna plate is considered negligible. The impedance of the length of wire connecting the circular plate to the BNC connector is largely dominated by the resistive and inductive components. Thus the impedance of the wire is given by $R_w + sL_w$, where R_w is the resistance and L_w is the self inductance. The wire resistance is considered negligible (measured less than 1 $m\Omega$ and the self inductance at 9 nH. Thus the impedance of the wire at 30 MHz, is 1.7 Ω. This is less than the impedance of the loads to be connected to the antenna (discussed later) and can thus be neglected. The length of co-axial cable used to connect the sensor to the load is 10 m long standard RG-58 co-axial cable, with a nominal capacitance of $100pF/m$ and an impedance of 50 Ω. The cable has the largest parasitic capacitance of all the non-ideal elements. The cable has a total capacitance of 1 nF, which is much smaller than the smallest integration capacitor used.

The sensor can be configured to measure either the electric field derivative

or the electric field by applying various loads [22]. In this experiment however the sensor was setup as a field sensor.

2.4.3 Electric Field Sensor Using Passive Integration

Assuming the load impedance applied to the sensor is much larger than the source impedance of the antenna itself the sensor output is a current proportional to the electric field derivative $\frac{dE_z}{dt}$. In order to use the output from the sensor effectively the load needs to be chosen carefully. Most basic recording equipment, such as oscilloscopes, essentially record the voltage over a large (1 $M\Omega$) or small impedance (50 Ω). It is preferential to choose a load that can provide a voltage proportional to the electric field from the current from the sensor. This requires integration of some sort. A capacitor conveniently provides this integration. The voltage from a capacitor is defined by Equation 2.14.

$$V_c = \frac{1}{C} \int i(t)dt \tag{2.14}$$

If a capacitive load, C_{int} is applied, the sensor capacitance is in parallel with the load capacitance. In which case the final impedance $Z_f = Z_l || Z_s$ can be described by Equation 2.15. Typically the capacitance of the load is in the range of tens to hundreds of nano-farads.

$$Z_s = \frac{1}{sC_{eq}} = \frac{1}{s\left(C_{ant} + C_{int}\right)} \tag{2.15}$$

Since every capacitor will have some form of leakage current, which is not necessarily linear, a resistor is placed in parallel with the capacitor to form a known discharge current which is larger than the non-ideal leakage current. Since the sensor will be connected to some recording instrument, in this case an oscilloscope, which has a defined impedance of typically 1 $M\Omega \pm 2\%$ and 15 pF, the effect of the equipment on the system dynamics needs to be considered [23]. The capacitance of the equipment is several orders of magnitude smaller than the load capacitance, C_{int}, and thus neglected. The measurement equipment is modelled as a resistor, R_{eq}. The final impedance Z_f on the current source of the sensor can be defined as follows

$$Z_f = Z_{C_{eq}} || Z_{R_{eq}} = \frac{R_{eq}}{sR_{eq}C_{eq} + 1} \tag{2.16}$$

Equation 2.16 applied to Equation 2.9 provides the output voltage from the sensor as a voltage $v_E(t) \leftrightarrow V_E(s)$, proportional to the electric field $E_z(s)$.

$$V_E = I\left(s\right) Z_f = \left\{\epsilon_0 A_{plate} s E_z\left(s\right)\right\} \left\{\frac{R_{eq}}{sR_{eq}C_{eq} + 1}\right\} \tag{2.17}$$

Dividing the numerator and denominator of the equation by $R_{eq}C_{eq}$, simplifies the equation further.

$$V_E\left(s\right) = \frac{\epsilon_0 A_{plate} E_z\left(s\right)}{C_{eq}} \frac{s}{s + \frac{1}{R_{eq}C_{eq}}} \tag{2.18}$$

The fraction on the right side of Equation 2.18 is recognisable as a single order high pass filter with a $-3\ dB$ point, ω_0, defined by Equation 2.19.

$$\omega_0 = \frac{1}{R_{eq}C_{eq}} \tag{2.19}$$

Therefore if the significant information of the electric field sensor exceeds this cut-off frequency ω_o such that $\omega >> \omega_0$ the output voltage from the sensor can be reduced to

$$V_E\left(s\right) = \frac{\epsilon_0 A_{plate}}{C_{eq}} E_z\left(s\right) \tag{2.20}$$

Therefore if a voltage $v_E(t)$ is recorded it can be used to infer the observed electric fields, $E_z(t)$, incident on the sensor by Equation 2.21.

$$E_z\left(t\right) = \frac{C_{eq}}{\epsilon_0 A_{plate}} V_E(t) \tag{2.21}$$

In the measurements performed the smallest integration capacitor and the smallest resistor used is 200 nF and 0.5$M\ \Omega$ respectively. Therefore the largest high pass bandwidth as defined by Equation 2.19 is 1.6 Hz. Thus the sensor can accurately measure the components of electric field changes faster than 100 Hz.

2.4.4 Passive Integrator Construction

Passive integration can be easily accomplished by using a single capacitor. The value of the capacitor needs to be carefully chosen based on several criteria. Firstly the value of the capacitor needs to be large enough such that the parasitic capacitances can be neglected. Secondly from Equation 2.21 the lower the value of the capacitor, the higher the output voltage of the sensor. The output voltage from the sensor should be high enough such that the signal voltage of the information is larger than the noise from the digitisation process or any other noise source. Additionally the signal must be of a high enough magnitude to be captured reliably and with enough resolution by the oscilloscope.

For this experiment the load capacitor was chosen so that the output signal is just large enough to trigger the oscilloscope. The resultant signal has a small signal voltage, which is just bigger than the voltage of the noise of the oscilloscope used.

For the flashes captured during the month of November the load capacitor was 200 nF. This capacitor was constructed in an aluminium enclosure by using eight 100 nF 1206 sized SMD X7R ceramic capacitors (two banks of four parallel capacitors in series) mounted on a piece of strip veraboard as shown in Figure 2.5(a). The 500 nF capacitor was constructed using the same technique, but different capacitors (20x 0603 ceramic X7R). Both capacitive loads were housed in aluminium enclosures, which were lined with paper (80 gm^{-2}) to avoid short circuits.

Since real capacitors can consist of non-ideal elements like inductance and resistance, the behaviour of the capacitors at high frequencies can differ from the ideal capacitor model. The capacitor loads were then exposed to a frequency sweep to ensure ideal operation and to measure the actual capacitance for various frequencies up to 5 MHz. The frequency sweep was performed with an Atten ATF05C arbitrary waveform generator. The capacitances of the capacitive loads were therefore calibrated to be 184 nF for the 200 nF load and 460 nF for the 500 nF load.

This passive integration technique was calibrated for, with the sensors,

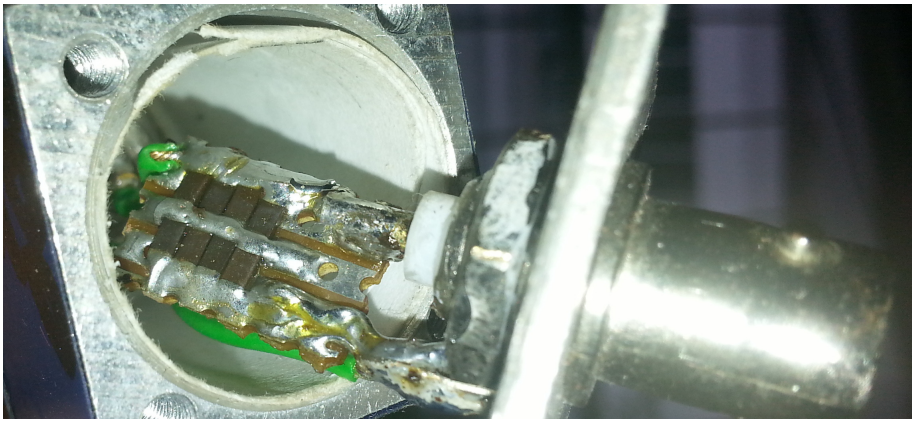

(a)

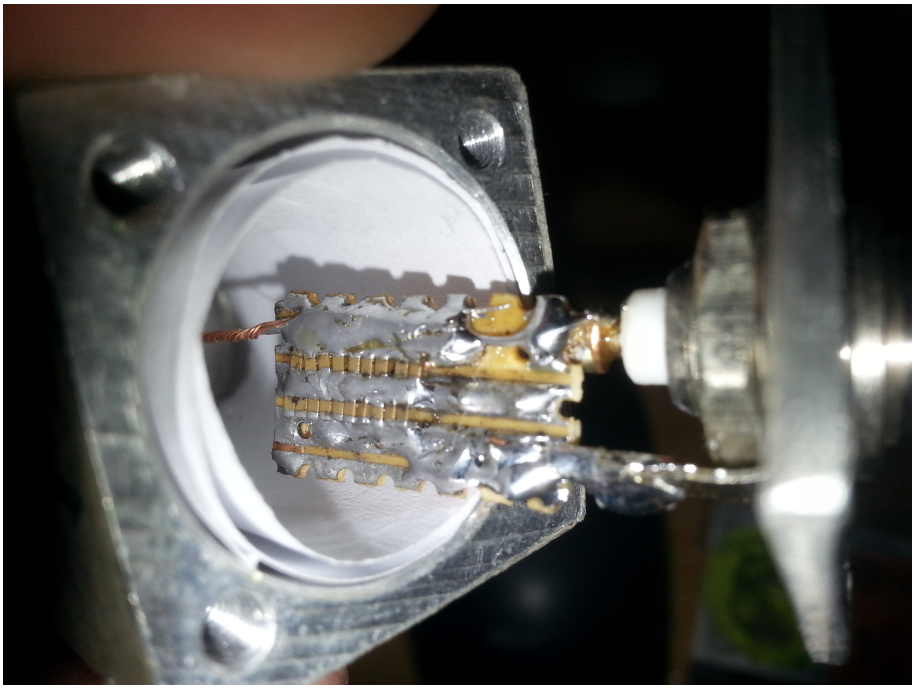

(b)

Figure 2.5: Internal view of 200 nF (2.5(a)) and 500 nF (2.5(b)) passive integrator loads showing construction of the load using 100 nF 1206 X7R and 0603 X7R ceramic capacitors respectively. The aluminium enclosures are lined with 80 gm^{-2} paper.

load-boxes and cables used in the final experiment (see Appendix A).

2.4.5 Active Integration

Since the integration of the current from the sensor as described above is performed solely by a passive circuit component, it is termed passive integration. The load capacitor is in parallel with the sensor plate. Therefore any voltage over the capacitor results in a voltage formed between the sensor plate and sensor frame. Ideally the sensor plate is short circuited to the sensor frame and the current between the sensor frame and sensor plate is measured. This is achieved by the use of an active integrator.

Active integration is achieved by using an operational amplifier in an integrator configuration. This presents a load to the source with an impedance similar to a short-circuit, through op-amp action. The operational amplifier will buffer the output from the sensor driving any loads such as the measurement equipment and the cable accurately.

There are undesirable effects of using an operation amplifier. Firstly any offset in the input stage of the operational amplifier will get integrated, which generally results in a large DC component in the output leading to clipping of the amplifier output. Although this offset may be compensated for, variations in the operational temperature for example can lead to changes in this offset negating the compensation, due to the high integrator sensitivity required. This effect can be mitigated by using a resistive element in the feedback loop of the amplifier [24].

Finally a stable power source is needed for this integration technique, which will need to be switched on when the system is armed.

2.4.6 Practical Considerations

The sensor was designed to avoid any conditions where rain water could form a conductive path between the sensor plate and sensor frame. There are two locations at risk of forming conductive paths. The first location is the annular gap, where surface tension could result in a drop of water connecting the plate to the frame of the sensor across the annular gap. The other location at risk of conduction is across the nylon bolts that support the

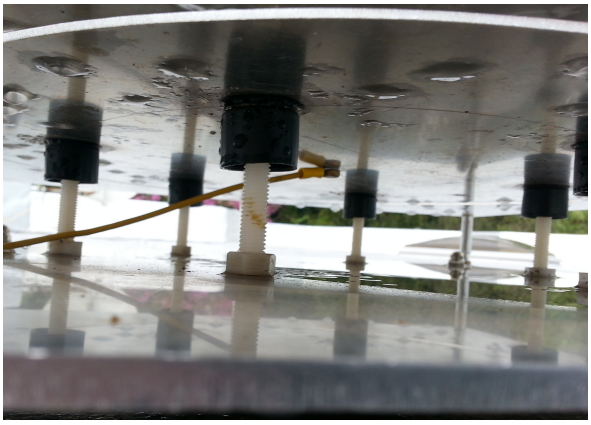

Figure 2.6: Bottom of sensor plate after a rainstorm. The plastic caps on the top of the nylon bolts keeps the tops of the nylon bolt dry.

sensor plate. In the latter scenario surface tension of the water could result in water accumulating on the bottom of the sensor plate and eventually flowing down the bolts resulting in a conductive path. This was mitigated by the use of plastic caps at the top of the nylon bolts as shown in Figure 2.6. Upon inspection of the sensor after a rainstorm when Figure 2.6 was photographed it was noted that the top of the nylon bolts were dry.

2.5 Sample Post Processing

The electric fields recorded by an oscilloscope suffer from several parasitic effects. Firstly the resistive component of the measurement equipment produces an RC decay in the measurement. Secondly the limited resolution of most oscilloscopes reduces the accuracy of the measurement. The oscilloscopes used in this study all had a vertical (voltage) resolution of 8 bits and relatively large noise. Both of these effects can theoretically be sufficiently negated by the use of appropriate post processing of the samples.

2.5.1 Filtering

Data from digital storage oscilloscopes is often low resolution, but oversampled. Generally the effective number of bits of an oversampled signal, increases by one bit, by oversampling by a factor of four. This is demonstrated

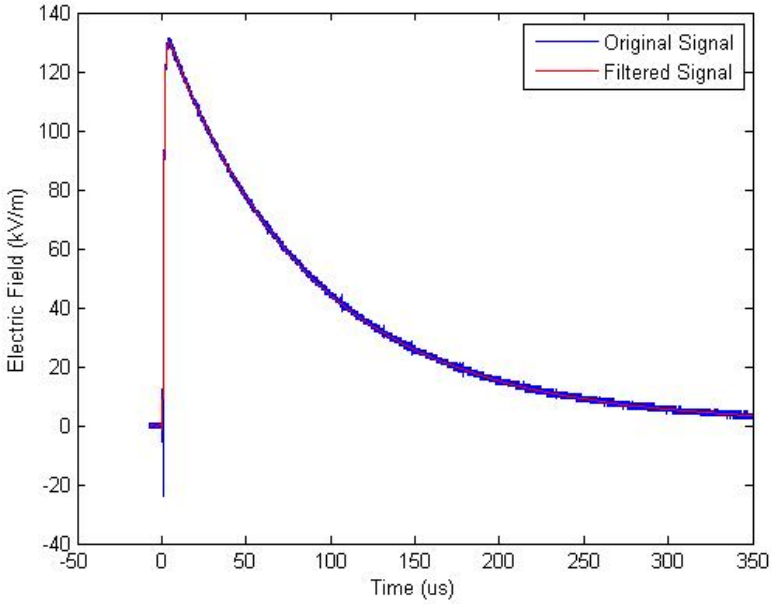

(a)

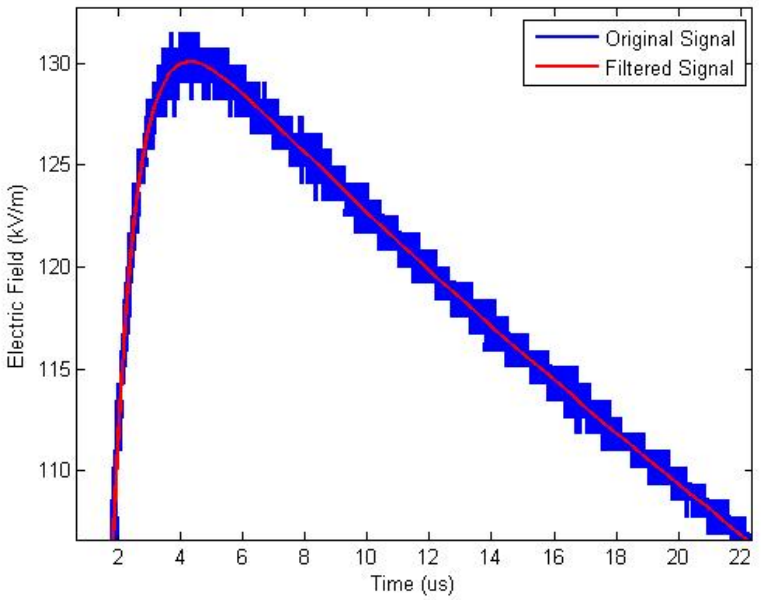

(b)

Figure 2.7: Modified $1.2/50\mu s$ impulse waveform. The original sampled signal is shown in blue, the signal filtered by a phaseless 8^{th} order 1 MHz low-pass filter is shown in red.

by Equation 2.22 [25].

$$f_{os} = 4^w f_s \tag{2.22}$$

Where f_{os} is the oversampled frequency, f_s is the original sampling frequency requirement and w is the number of additional bits of resolution required.

Once the oversampled signal has been acquired, it is possible to extract the higher resolution signal via several methods. The choice of method depends on the noise sources. One technique is to average the samples over a fixed interval. For instance if the signal is oversampled by a factor of 256, then an average will be taken every 256 samples. An alternative is to use a low pass filter, being careful to consider any affects of the filter on the phase of the measurement. There are practical limitations to this approach that are largely determined by the noise, accuracy and effective resolution of the measurement equipment.

Since the electric field waveforms from lightning events are time based signals care must be taken to avoid affecting the phase of the recordings. As such the filter used is a digital phase-less filter. The phase of the samples is not affected by a digital phase-less filter. The only considerations of the filter design is the cut-off frequency and the filter order. A digital phase-less filter is implemented by applying a digital filter in the forward direction and then applying the same filter on the results from the first filtering stage in the backward direction. The results from this filter has zero phase distortion and the magnitude modified by the square of the filters magnitude response [26].

As shown in Figure 2.7(a), the low pass filter extracts the higher resolution data that can be used reliably in further analysis. For example consider the modified 1.2/50 μs impulse measured with an 8-bit resolution oscilloscope, shown in in Figure 2.7(a). This waveform was passed through an eight pole phase less filter with a cutoff frequency of 1 MHz. This demonstrates the lack of phase distortion present in the signal as well as the extracted numerical data of a higher resolution than the original sampled signal. This is process is further analysed in Appendix A.

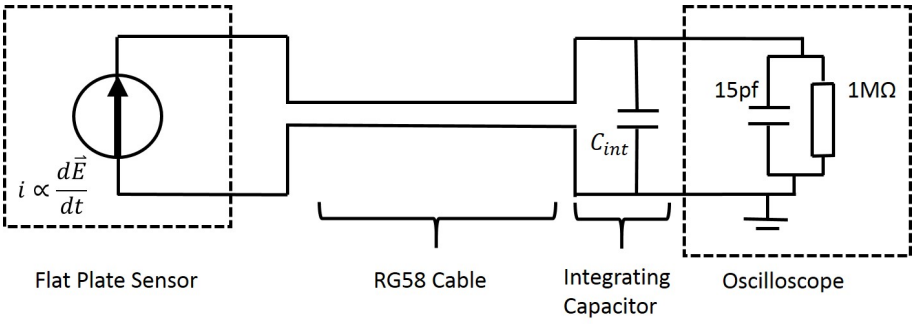

Figure 2.8: Diagram of sensor connection showing non-ideal elements of the oscilloscope input stage.

2.5.2 Reducing the RC decay

The other goal of the post-processing step is to reduce the effects of the RC decay. The RC decay occurs due to the presence of the discharge resistor defining a known discharge, shown in Figure 2.8. This resistor discharges the integrating capacitor C_{int} by a known amount, as opposed the unknown discharge inherent in real capacitors. Since the RC decay is accurately defined its effect can be modelled and compensated for. This process has been utilised in previous studies [16, 21].

This analysis will be performed in the Laplace domain.

For an ideal configuration, where the resistance of the oscilloscope is neglected, the capacitor C_{int} integrates the current $i(t) \leftrightarrow I(s)$ as defined in Equation 2.14, the Laplacian representation of the ideal case voltage V_{ideal} is as shown in Equation 2.23.

$$V_{ideal}(s) = \frac{1}{C_{int}} \frac{1}{s} I(s) \tag{2.23}$$

Considering the resistive element, R, in parallel with the integrating capacitor, the voltage in the from the resultant system which models the actual system, V_{actual}, is described by Equation 2.24

$$V_{actual}(s) = \frac{R}{RC_{int}s + 1} I(s) \tag{2.24}$$

Thus the voltage from the real system, V_{actual}, can be used to infer the

actual current, $I_{actual}(s)$.

$$I_{actual}(s) = \left\{ C_{int}s + \frac{1}{R} \right\} V_{actual}(s) \tag{2.25}$$

Substituting this result for $I_{actual}(s)$ into $I(s)$ of the ideal transfer function (Equation 2.23) yields the following result.

$$V_{ideal}(s) = \left(\frac{1}{C_{int}s}\right)\left(C_{int}s + \frac{1}{R}\right) V_{actual}(s) = \left(1 + \frac{1}{RC_{int}}\frac{1}{s}\right) V_{actual}(s) \tag{2.26}$$

This translates back into the time domain giving the correction equation utilised in this research, Equation 2.27.

$$V_{ideal}(t) = V_{actual}(t) + \frac{1}{RC_{int}} \int V_{actual}(t)\, dt \tag{2.27}$$

This equation matches that produced previously by Vladislav Mazur and Lothar H. Ruhnke ([16]) defining the time constant by the components in the circuit.

2.6 Lightning Stroke Current Inference from Electric Fields

It is possible using the models derived earlier to determine the electric field changes from the changes in the charge centre. Conversely it is possible to infer the change in charge from the changes in the electric field. Starting from Equation 2.2 and solving for the charge, q.

$$q = -E_z \frac{4\pi\epsilon_0}{H_c} \left[d^2 + H_c^2 \right]^{\frac{3}{2}} \tag{2.28}$$

The electric field sensor can detect the fast changes in the electric field. Therefore the electrical field derivative ($\frac{dE}{dt}$) can be measured. The instantaneous lightning current i_l is the rate at which the charge centre is discharged ($i_l = \frac{dq}{dt}$). Hence it is possible to infer the instantaneous lightning current, by Equation 2.29.

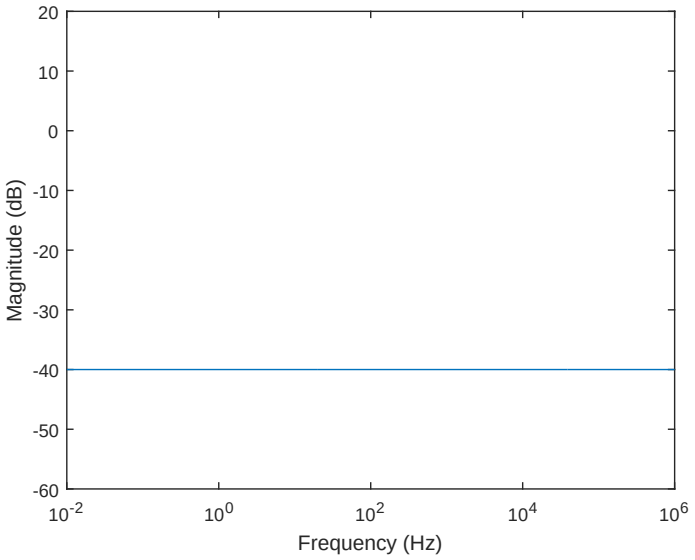

Figure 2.9: Bode magnitude plot for white noise, with a magnitude of -40dB.

$$i_l = \frac{dq}{dt} = -\frac{dE_z}{dt}\frac{4\pi\epsilon_0}{H_c}\left[d^2 + H_c^2\right]^{\frac{3}{2}} \tag{2.29}$$

Note that the negative sign implies as before that a positive electric field derivative implies a negative lightning stroke current. It is assumed that the charge centre and stroke path does not change. Therefore H_c and d are constant for a single lightning event. Note that the current is proportional to the electric field derivative.

2.7 Noise in Measurements

The inference of the lightning event current is dependant on the derivative of the electric field. The effect of measurement noise on the derivative is investigated in this section. For any real measurement system, there are several noise sources. Real analogue to digital converter circuits will introduce noise and distortion [27]. Digital storage oscilloscopes rely on analogue to digital converters to convert the analogue voltages to digital signals. For this reason analogue to digital converters are specified with an effective digital resolution. The resolution and noise performance can be improved by digital

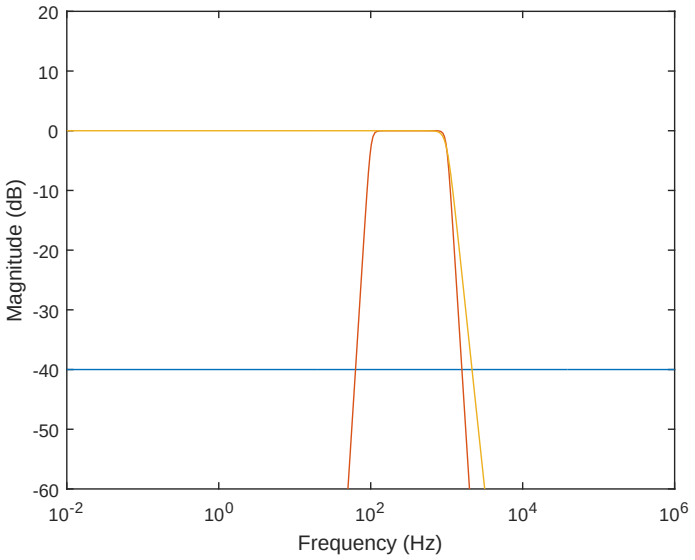

Figure 2.10: Bode magnitude plot with the white noise (blue), the information (100 Hz-1 kHz, Red) and the filter (1 kHz, Yellow)

post-processing [25]. The effect of the low pass filter to reduce the noise in the frequency domain will be demonstrated by means of an example.

For this analysis it will be assumed that all the noise sources can be adequately modelled as white noise. In the frequency spectrum white noise has a constant magnitude for all frequencies, shown in Figure 2.9. For this analysis the noise has a magnitude of $-40\ dB$. It is next assumed that the signal of interest has a magnitude of 0 dB and occurs within the 100-1000 Hz bandwidth. In order to reduce the noise using a low-pass filter a bandwidth of more than 1000 Hz, can be used. In the Figure 2.10 a bandwidth of 1 kHz was used for the filter. This filter will remove as much noise as is possible without significantly affecting the information. However if the information is in the 200-2000 Hz bandwidth, for example, the filter chosen before, 1 kHz, will affect the information as shown in Figure 2.11. Obviously the filter bandwidth can be increased to reduce this effect.

When a derivative is applied to the signal the noise is amplified, obscuring the signal. The transfer function for a derivative is $H(s) = s$ and a bode plot of the transfer function is shown in Figure 2.12. The bode plot

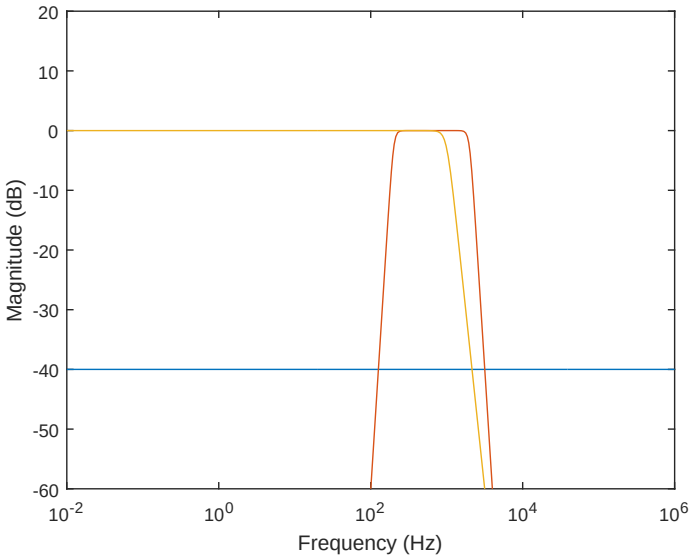

Figure 2.11: Bode magnitude plot with the white noise (blue), the information (200 Hz-2 kHz, Red) and the filter (1 kHz, Yellow)

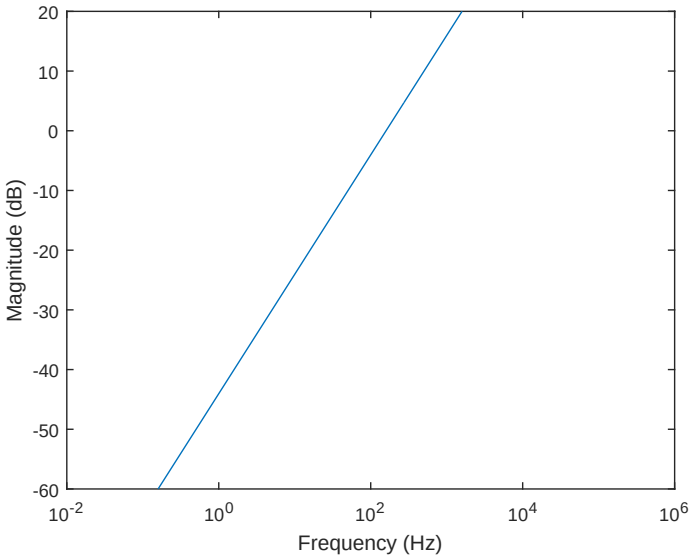

Figure 2.12: Bode magnitude plot for a derivative, with a gain of 0.001.

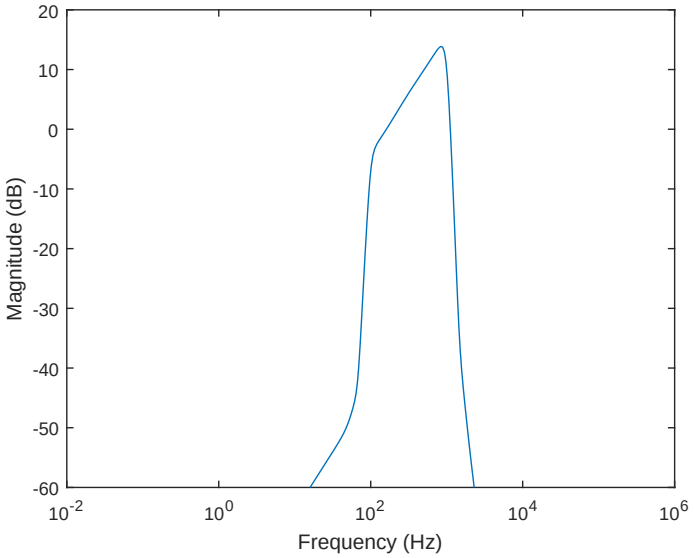

Figure 2.13: Bode magnitude plot of the resultant signal after a derivative is applied to the signal. The bandwidths of the information is 100 Hz-1 kHz, with a filter bandwidth of 1 kHz.

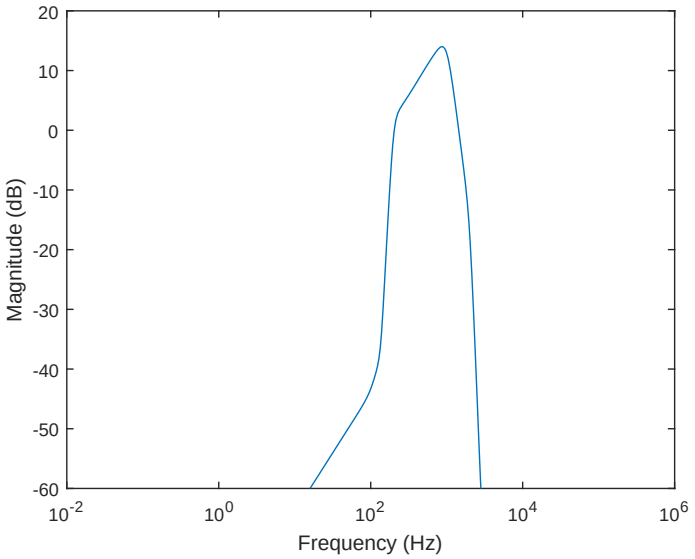

Figure 2.14: Bode magnitude plot of the resultant signal after a derivative is applied to the signal. The bandwidths of the information is 200 Hz-2 kHz, with a filter bandwidth of 1 kHz.

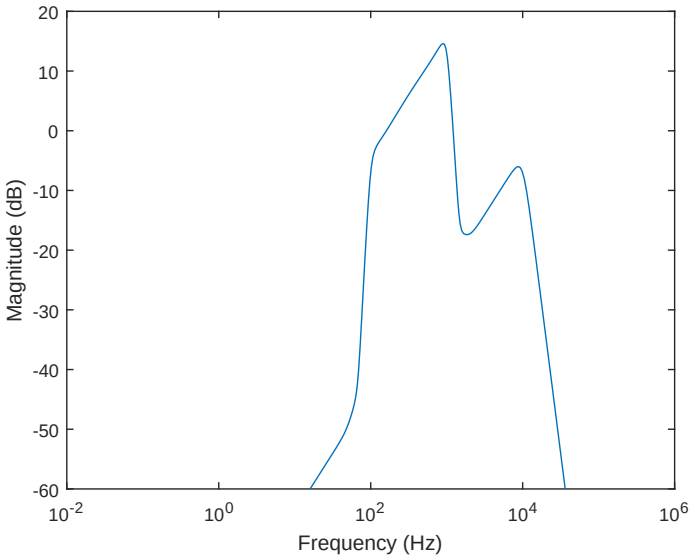

Figure 2.15: Bode magnitude plot of the resultant signal after a derivative is applied to the signal. The bandwidths of the information is 100 Hz-1 kHz, with a filter bandwidth of 10 kHz.

of the information combined with the noise following the application of the derivative for the two different information bandwidths (100 Hz-1 kHz and 200Hz-2 kHz) is shown in Figures 2.13 and 2.14. Figure 2.13 represents the best case for the resultant information. The higher frequencies are amplified more by the derivative as expected. Thus the high frequencies containing the information are of high importance. Figure 2.14 is missing some higher frequency information which significantly influences the resultant information. If the filter bandwidth is increased the resultant bode plot will look like that shown in Figure 2.15. With a higher filter bandwidth the noise is amplified by the derivative to a high magnitude.

Normally the signal magnitude (0 dB) is much larger than that of the noise (-40 dB). However when the derivative is applied the higher frequency noise is amplified by the derivative. If the filter bandwidth is too high the noise will have a larger magnitude than the information. If the filter bandwidth is too low then the filter will affect the information. In this example there does exist a case, where the filter bandwidth can be chosen in a way

such that the filter will eliminate as much of the unwanted noise, without affecting the information. This is the case in Figure 2.13.

However if the signal magnitude is not much larger than the noise, distinguishing the signal from the noise becomes difficult. Furthermore the effect of the derivative on the resulting signal may result in the noise being amplified to a larger magnitude than the signal itself.

2.8 Summary

This chapter presents the background theory behind the lightning discharge process in a cloud to ground lightning event. Within a thundercloud is a tripole of electric charges. The lightning event discharges one of these charge centres. The decrease in charge within the charge centre creates a change in the electric field. From the change in the electric field the change in charge can be inferred. This change in charge can be used to infer the instantaneous lightning stroke current. The change in the electric field is detected by a flat plate sensor. The presence of noise in the electric field measurement will influence the accuracy of the lightning current inferred from the electric fields recorded. This theory will be used in the next chapters as the theoretical foundation upon which the analysis is performed.

Chapter 3

Experimental Description

The theory needed to capture the electric field waveforms from a cloud to ground lightning event was presented in Chapter 2. The theory presented a means by which the instantaneous lightning current may be inferred from the electric fields recorded. This chapter presents the physical experimental system used to record the electric fields from a cloud to ground lightning event. The methodology used to obtain the electric field waveform is also shown. Thereafter the processes used to compensate for known measurement errors is presented. The technique by which the data from the Lightning Detection Network is correlated to the lightning event recorded is presented. Finally the means by which the instantaneous current of the lightning event is inferred from the electric field recording is detailed.

3.1 Overview

The sensors were placed on a rooftop in a suburban environment. The measurement setup was controlled by an operator. The electric fields observed by the sensor are extracted from the sensor voltage output. Firstly the resolution of the recorded waveform was increased by applying a low pass filter to the oscilloscope voltage data. The resistive discharge of the integrating capacitor due to the oscilloscope was then removed from the filtered signal. The resulting waveform was then multiplied by the gain of the sensor to obtain the electric fields observed by the sensor. The lightning current was

(a) (b)

Figure 3.1: Flat plate sensors on roof looking towards the North (3.1(a)) and South (3.1(b))

extracted from the electric field data. The process was repeated for multiple filter bandwidths. The inferred lightning current was compared to the lightning current recorded by the South African Lightning Detection Network.

3.2 Experimental Setup

This section describes the physical setup and methodology used to capture the electric field waveforms of the lightning events in Johannesburg during the summer of 2014/2015.

3.2.1 Location

The location chosen is in an area with a high lightning incidence which is also accessible for an operator. The sensors were placed on the top of a roof in a residential location in Victory Park, Johannesburg. The lightning incidence of Johannesburg is between $7.5 - 12$ flashes/km^2/year [2, 28]. The roof is earthed corrugated iron covered in polystyrene, wood and rubber. This forms a large highly conductive plane for the antenna reducing field concentration and any horizontal electric field components [12]. The sensor was connected to the load box and recording instrumentation by a 10 m length of RG-58 cable, that was used in the calibration tests (see Appendix A). Two sensors

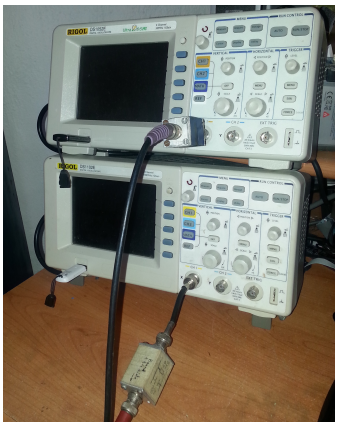

Figure 3.2: The two oscilloscopes used to capture the recordings during the experiment. The load boxes are the small boxes located very close to the oscilloscope's input.

were placed approximately 5 m apart.

3.3 Measurement Equipment

In order to measure the output from the sensors, two digital storage oscilloscopes (DSO's) were utilised: a Rigol DS1052E and a Rigol DS1102E. The DS1052E and DS1102E are effectively the same oscilloscopes but with a analogue bandwidth of 50 MHz and 100 MHz respectively. These oscilloscopes were chosen as they have measurement noise of better than -35 dB when measuring a 570 mV_{rms} 1 kHz sine wave [29].

In order to capture the most number of strokes as possible, only one sensor was used and connected to either of oscilloscopes. Thereby one oscilloscope is available to record the electric fields from a lightning event, while the other is storing the data from a previous lightning event to non-volatile storage.

The oscilloscopes were setup with a horizontal 50 ms per division and a vertical 50 mV per division. During the scope of this experiment all inputs had an impedance of 15 pF$\|$ 1 $M\Omega$.

3.3.1 Measurement Equipment Location

The oscilloscopes used were placed in the room directly below the sensors. Each oscilloscope was connected to an online uninterrupted power supply

(UPS) to provide constant power to the oscilloscope despite the power fluctuations that occur due to the lightning. These UPS's provided a connection to the mains earth. The mains earth in the house is supplemented by the steel wiring conduits. Thus the oscilloscopes are grounded. The corrugated iron roof, burglar bars and iron mesh used in the walls, provides sufficient electromagnetic shielding for the oscilloscopes.

3.3.2 Measurement Acquisition Strategy

The recording instruments were triggered by the signal itself. When the signal changed by a high enough magnitude the equipment would be triggered. This was achieved on the Rigol DS1102 and DS1052 Oscilloscopes by using the built in functionality of the oscilloscope. The sensor signal is AC coupled to the trigger, with a bidirectional slope threshold of 8.00 mV. The operator ensured that the triggering of the oscilloscope coincided with some form of ground truth event such as a light flash and/or thunder.

The system was armed following the observation of lightning indicators. These indicators include lightning flashes, thunder and nearby lightning reported by the South African Lightning Detection Network.

The operator of the recording system had access to an internet connection and hence could get the time of the stroke via the website *onlineclock.net*. Delays in the recording process meant that the recorded event time is accurate to ± 30 seconds.

3.3.3 Calibration and Validation

The flat plate electric field sensor, connecting cable and load used during the experiment was calibrated. Details about the calibration of the sensor is contained within Appendix A. The sensor setup was validated to ensure that the fields observed by the sensor were in-fact those of the lightning event. This was done by using a second sensor with its own independent measurement system. The details of the validation experiment are contained in Appendix B.

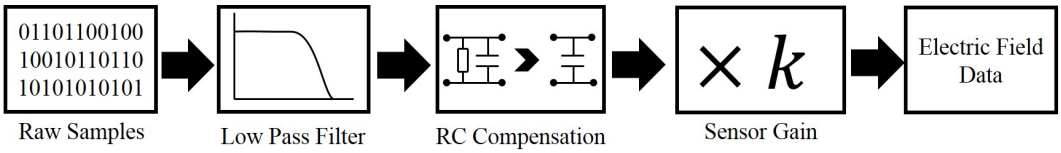

Figure 3.3: Process diagram demonstrating how the samples from the oscilloscope, as voltages, were processed to obtain the electric field data.

3.3.4 The South African Lightning Detection Network

The SALDN is a lightning location system comprising of 20 Vaisala LS7000 sensors (19 sensors in South Africa and one in Swaziland). It was commissioned by the South African Weather Service (SAWS) and has been operational since January 2006 [2, 30]. This system has been the study of various accuracy tests, which compare ground truth data to the output from the system [31, 32]. This system is used to determine the approximate location of any recorded lightning event by comparing the time of the recording to the detected lightning events. These distances are vital to the application of the various models of the lightning event used in this experiment. The data from the South African Lightning Detection Network, is a list of lightning strokes detected. The raw data from the lightning detection network contains the time, GPS co-ordinates and peak current of all detected lightning strokes.

3.4 Methodology

The methodology by which the electric fields are processed is detailed in this section. The recorded electric fields are then used to infer the lightning event electric current. The filter applied to the recorded electric fields is adjusted to observe the effects of the noise on the inferred lightning currents. The distance from the sensor to the lightning event is obtained from the South African Lightning Detection Network.

3.4.1 Signal Processing

The first step of processing any of the recordings from the electric field sensors is to extract the electric fields observed by the sensors. The samples, in the form of the voltage measured by the oscilloscope are first processed by

a low pass filter to extract a higher resolution of data from the samples (Section 2.5.1). The filter is a 4^{th} order digital phase-less filter (effectively an 8^{th} order filter). These samples are then processed to remove the RC decay (Section 2.5.2) then multiplied by the sensor gain (Equation 2.21) to get the electric fields observed by the sensor (Section 2.4.3). This process is demonstrated in Figure 3.3.

Implementing RC Compensation

To apply Equation 2.27 to the recorded signals in the discrete time domain, a Riemann sum is used to discretely evaluate the integral. This produces Equations 3.1 and 3.2 which are applied to the recorded samples to implement the RC decay compensation. The RC decay compensation is applied after the filter used to increase the resolution.

$$V_{ideal}[n] = V_{actual}[n] + V_{Integral}[n] \tag{3.1}$$

$$V_{Integral}[n] = V_{Integral}[n-1] + V_{actual}[n]\frac{\Delta t}{RC_{int}} \tag{3.2}$$

Any DC offsets in the measurement must be removed before the integration process is applied. If not removed any DC offset will result in an erroneous ramp from the integration process. Sources of DC offsets include an uncalibrated offset in the oscilloscope or initial conditions for example. For this reason, where possible an average of the first ten thousand samples were taken to measure the offset. The DC offsets were only removed from the samples just before the RC decay compensation process.

3.4.2 Correlating to LDN Data

The time of the recording is noted by an operator resulting in a measurement uncertainty of ± 30 seconds. Closer lightning strokes produce larger electric field changes (Equation 2.2) making it more likely that the closest lightning events trigger the oscilloscopes. The following procedure is followed to match a recorded lightning event to the data from the South African Lightning Detection Network.

1. All lightning events in a square area, with 20 km sides, with the sensor

location in the centre, for the minute preceding and proceeding the recorded lightning event are extracted from the LDN.

2. The GPS co-ordinates of these events are then reduced to distances from the sensor, using the Haversine Formula [33].

3. The furthest lightning strokes are removed. This is decided by first removing all strokes at distances of greater than 10 km away. This distance is reduced if there are many lightning strokes in the resulting data.

4. The lightning strokes are grouped into their individual events based on the GPS co-ordinates.

5. The lightning events are then compared to the electric field data. Factors such as number of strokes, time between strokes and polarity (by Equation 2.2) are compared. By this stage there are usually less than 3 events from the LDN under scrutiny.

6. If the earliest event is also the closest, this event is assumed to be the event recorded. Other factors such as the operator's notes of the time between the visible flash and the audible sound of thunder are considered.

This process has proved effective at narrowing the data down from the lightning detection network. Occasionally other factors and data from the electric field data would be compared to the lightning detection network data, however this is very case specific. This lightning detection network data is required for the distance scaling of the electric fields to the actual magnitudes of the charge (see Equation 2.2).

3.4.3 Inferring Lightning Current

The lightning current can be inferred from the electric field information using the distance of the sensor from the lightning event as a scaling factor. The distance of the sensor from the lightning event is taken from the South African Lightning Detection Network. The lightning peak current and polarity is

also available from the lightning detection network data. At this stage of processing the electric fields recorded by the sensor has been filtered and the resistive decay compensated for. The filter bandwidth is swept from 1.5 kHz to 50 kHz and for each frequency the lightning current from the electric fields is calculated. Equation 2.29 is used to infer the lightning event current from the recorded electric fields. The peak inferred current for each filter bandwidth is compared to each other.

3.5 Summary

The setup and operation of a measurement system used to record the electric fields from cloud to ground lightning has been presented.

The system utilises flat plate electric field sensors to measure the electric fields radiated from the lightning events. The waveforms from these sensors are recorded by Digital Storage Oscilloscopes which are controlled by an operator. The oscilloscopes chosen have a low resolution and a high noise level.

The electric fields recorded go through two stages of post-processing. The first stage is a low pass filter to reduce the measurement noise in the recording. The low pass filter also increases the resolution of the recorded electric fields. The second stage compensates for the resistive decay inherent in the measurement instrumentation.

The recording is correlated to a lightning event recorded by the South African Lightning Detection Network. The distance of the lightning event from the sensor is obtained from the lightning detection network. The peak lightning current is also measured by the Lightning Detection Network. The lightning current can be inferred from the electric fields recorded using the distance of the sensor from the lightning event as a scaling factor. The peak lightning current inferred from the electric field data for a range of filter frequencies is calculated. This methodology is applied to the electric fields radiated from a lightning event shown in the next Chapter.

Chapter 4

Case Study

The theory as to how a lightning event results in a change in the electric fields is presented in Chapter 2. From this theory the instantaneous current can be inferred from the changes in the electric field. Using this theory the methodology to obtain the electric field waveform and infer the lightning current from the electric fields was presented in Chapter 3. In this chapter the methodology presented in Chapter 3 is applied to the electric fields radiated by a lightning event. This event was recorded on the 3 January 2015 13h57m22. The effects of the measurement noise on the lightning current inferred from the electric fields is investigated.

4.1 Overview

The electric fields for a lightning event that occurred on the 3 January 2015 13h57m22 are used to infer the lightning current for that lightning event. This lightning event was correlated to an event recorded by the South African Lightning Detection Network. The distance of this stroke from the sensor was recorded by the South African Lightning Detection Network to be 4.28 km. The electric fields were recorded with an oscilloscope which has a low resolution and a high measurement noise. The recorded electric fields are first passed through a low pass filter. Several frequencies are used as the filter bandwidth. The resultant waveforms from each filter frequency are then processed to reduce the resistive decay. The lightning current is then inferred

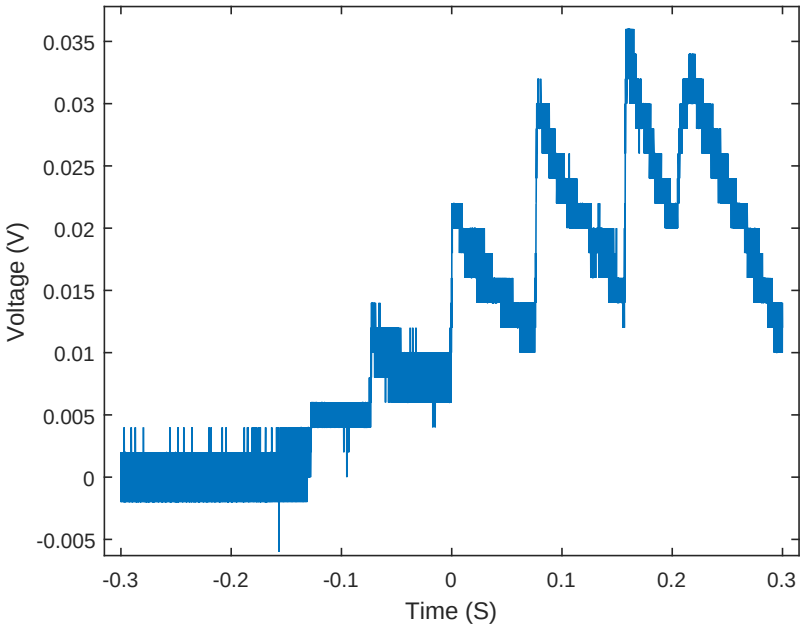

Figure 4.1: Voltage output from the sensor vs time recorded 3 January 2015 13h57m22.

from each waveform.

It is observed that it is not possible to accurately infer the absolute lightning current from the recorded electric field used. The measurement noise of the recording instrumentation is to large compared to the low signal voltage from the sensor.

4.2 The Recorded Waveform

The recorded waveform from the sensor without any processing for the cloud to ground lightning event used in this case study is shown in Figure 4.1. This recording coincided with the visual and auditory proofs of a cloud to ground lightning event. The time between the lightning flash and thunder was about 14 seconds. This corresponds to an approximate distance of 4.8 km between the sensor and the lightning event (speed of sound $\approx 0.34\ km.s^{-1}$) [17].

From the electric field information alone the number and polarity of lightning strokes can be inferred. There appear to be 6 negative lightning strokes

that occurred during this lightning event. The relative charge transferred during each stroke can also be inferred by observing the differences in the steps in the electric fields (ΔE, Equation 2.3). By this manner it is determined that the most charge was transferred during the second last stroke.

There are 21 discrete steps in the recorded voltage. The noise appears to have a magnitude of three to four discrete steps. There are 256 discrete values available in the digital 8 bit resolution system used. This results in significant resolution based noise interference. The signal was sampled at 1.75 MSps. The voltage range used in this experiment is set by the oscilloscope software. The voltage per division was set to 50 mV/div.

4.3 Applying the Methodology

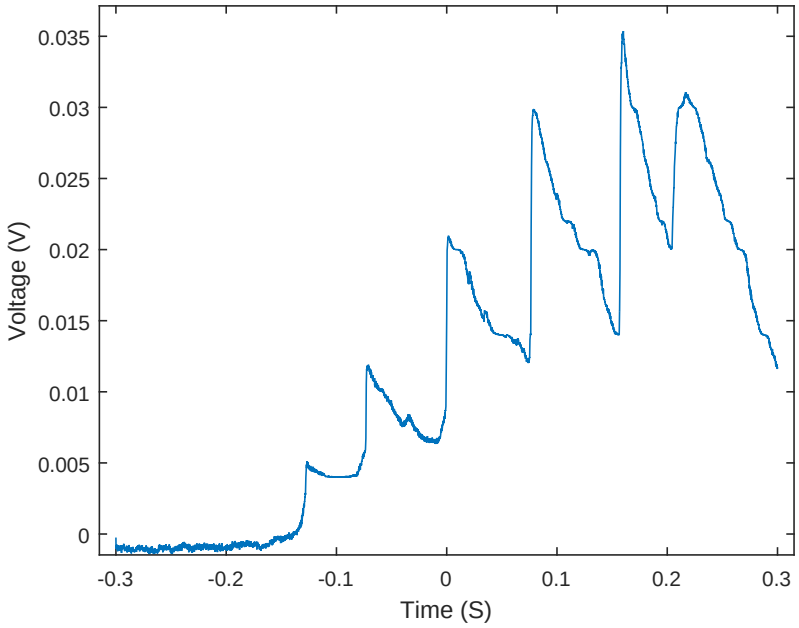

Figure 4.2: Filtered voltage output from the sensor vs time recorded 3 January 2015 13h57m22. The filter bandwidth for this waveform is 7 kHz

The methodology detailed in Section 3.4 is applied to the recorded waveform.

4.3.1 Signal Processing

Firstly the filter was applied to the electric field waveforms. Several filter bandwidths from 1.5 kHz to 50 kHz were used. The resultant waveforms from each filter were stored for the next stage of processing. A typical filtered waveform, with a bandwidth of 7 kHz is shown in Figure 4.2. It is observed that as desired the noise is significantly reduced. The fast positive changes, corresponding to the lightning events have a longer rise time (from $\approx$ 120 μs to 150 μs for the second last impulse). It is however noted that each individual step corresponding to an individual lightning stroke in the event is more distinguishable. It is easier to locate the 10 % and 90 % points on the filtered waveform for the rise time calculation.

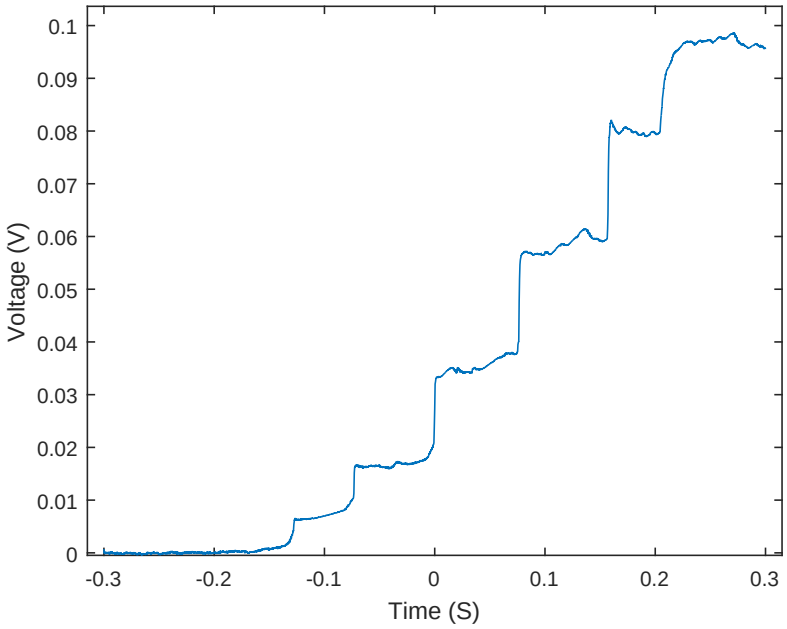

Figure 4.3: Compensated voltage output from the sensor vs time recorded 3 January 2015 13h57m22. The filter bandwidth of this waveform is 7 kHz.

Secondly Equation 3.1 was applied to the filtered waveforms compensating for the resistive decay in the measurement. Figure 4.3 shows the waveform from Figure 4.2 following the compensation process. From this example the

exponential decay present in Figure 4.2 is sufficiently negated.

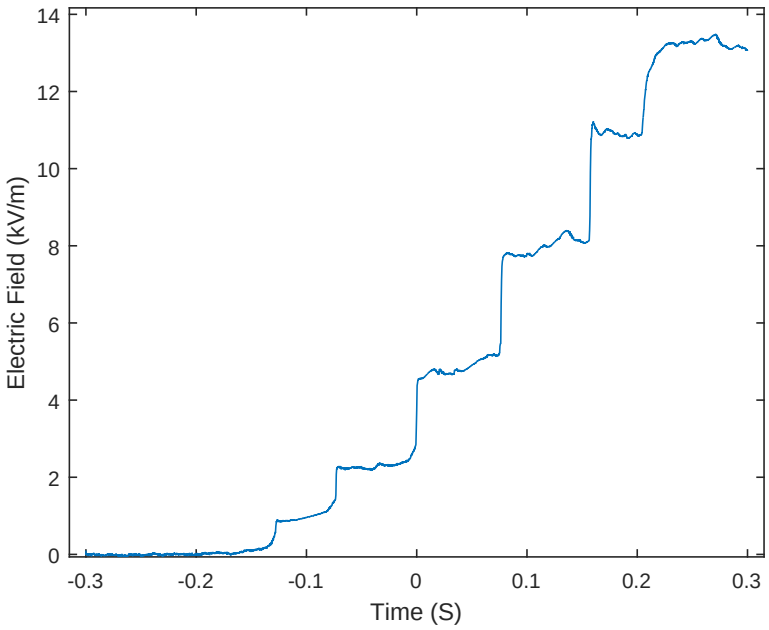

Figure 4.4: Electric fields vs time recorded 3 January 2015 13h57m22. The filter bandwidth of this waveform is 7 kHz.

Finally the compensated voltage from Figure 4.3 is multiplied by the sensor gain to obtain the electric fields observed by the flat plate electric field sensor. The resultant field plot for the lightning event is shown in Figure 4.4. It is noted that all the significant changes to the electric field are positive, implying that only negative strokes occurred (Equation 2.29).

4.3.2 Correlating the Lightning Detection Network Data

The recording used in this case study was recorded during a intense lightning storm with 36 lightning events being recorded by the lightning detection network within a 20 km radius in 5 minutes. The Lightning Detection Network data was reduced to all entries that occurred within ±30 seconds of the recording and within a range of 7 km, based on the approximate distance noted by the operator. The entries from the lightning detection network for lightning activity within a 7 km radius and within ±30 seconds are located

Table 4.1: Dates and times of all recordings from the lightning detection network of negative lightning cloud-to-ground events that occurred at distance of less than 7 km from the sensor. These entries are limited to those that occurred within ±30 seconds of 3 January 2015 13h57m22.

Date and Time	Ip (kA)	Distance (km)
01/03/2015 13:57:12.900	-16.00	5.60
01/03/2015 13:57:13.000	-18.00	5.28
01/03/2015 13:57:13.100	-24.00	4.28
01/03/2015 13:57:13.100	-30.00	4.28
01/03/2015 13:57:13.200	-32.00	4.28
01/03/2015 13:57:13.200	-6.00	6.76
01/03/2015 13:57:13.300	-6.00	4.32
01/03/2015 13:57:13.300	-8.00	4.28

in Table 4.1. The discrepancy in the time of the recording and the time from the Lightning Detection Network, about 9 seconds is attributed to the process delay of the operator. The closest lightning event which coincidentally had the highest current reported by the Lightning Detection Network probably resulted in the largest electric field changes (Equation 2.3). Thus it is more likely that the oscilloscope was triggered by the closest lightning event. Thus the event recorded was most likely the 4 detected events that occurred at a distance of 4.28 km away from the sensor.

4.3.3 Inferring Lightning Current

Using the distance of the lightning event from the sensor the lightning current can be inferred. The charge centre height (used as H_c in Equation 2.29) is assumed to be 7 km, which is the same as that for Florida [12]. The peak current calculated from the electric fields for each filter bandwidth is shown in Figure 4.5. It is noted in Figure 4.5 that the peak value is not constant for any range of filter cut-off frequencies.

The inferred currents are shown for various filter cut-off frequencies in Figures 4.6(a) to 4.7(b).

The lowest filter cut-off frequency that could be implemented stably is 1.5 kHz. The current inferred from the electric fields of the lightning event

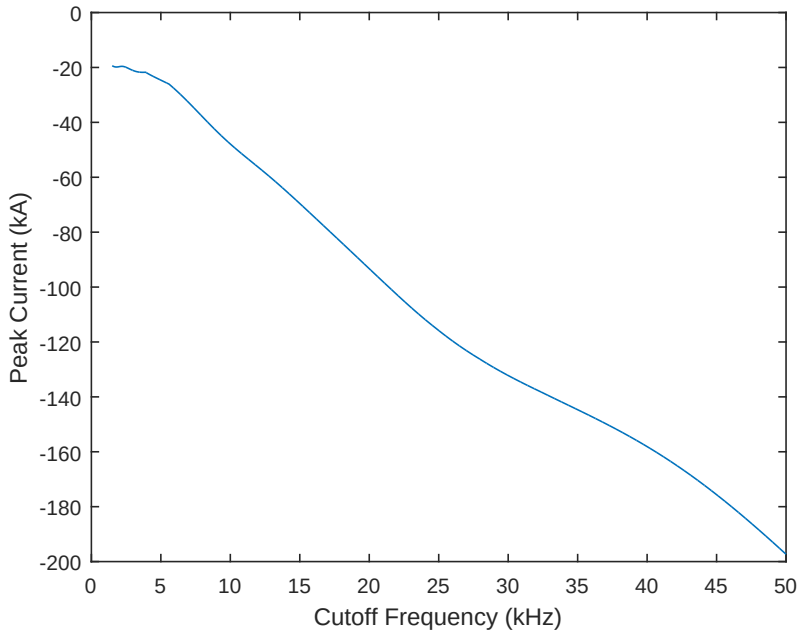

Figure 4.5: Peak inferred stroke current vs Low-pass filter cut-off frequency for the lightning event recorded 2015/01/03 13:57:22.

with a cut-off frequency of 1.5 kHz is shown in Figure 4.6(a). The signal when there is no lightning activity is approximately at the 0 kA level, which is expected. The strokes can be easily identified and the peak value for each stroke is clear to obtain. The largest positive impulse of 1.3 kA is considered erroneous, as no significant negative electric field changes were noted in Figure 4.4 (Equation 2.3). The times for each of the stroke peaks is used to identify the strokes in the comparisons with other filter bandwidths below.

Increasing the cut-off frequency of the filter slightly to 2 kHz, results in a significant change to the current waveform. The current waveform, inferred from the electric fields recorded of the lightning event is shown in Figure 4.6(b). The noise around the 0 kA level has increased. The peak current of the individual lightning events has increased compared to the current waveform with a filter cut-off of 1.5 kHz (Figure 4.6(a)). The increase in peak currents of a lightning stroke relative to the other strokes is not constant.

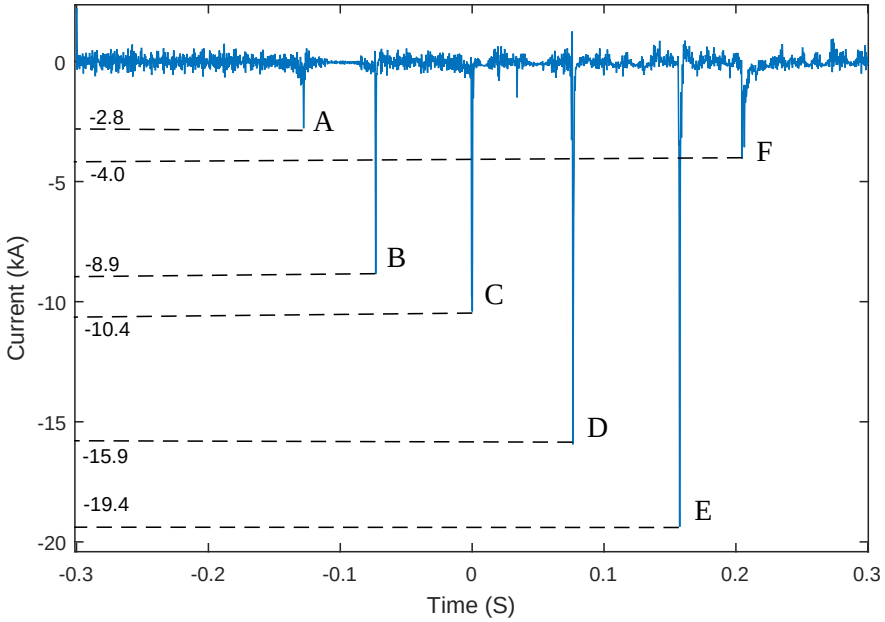

(a)

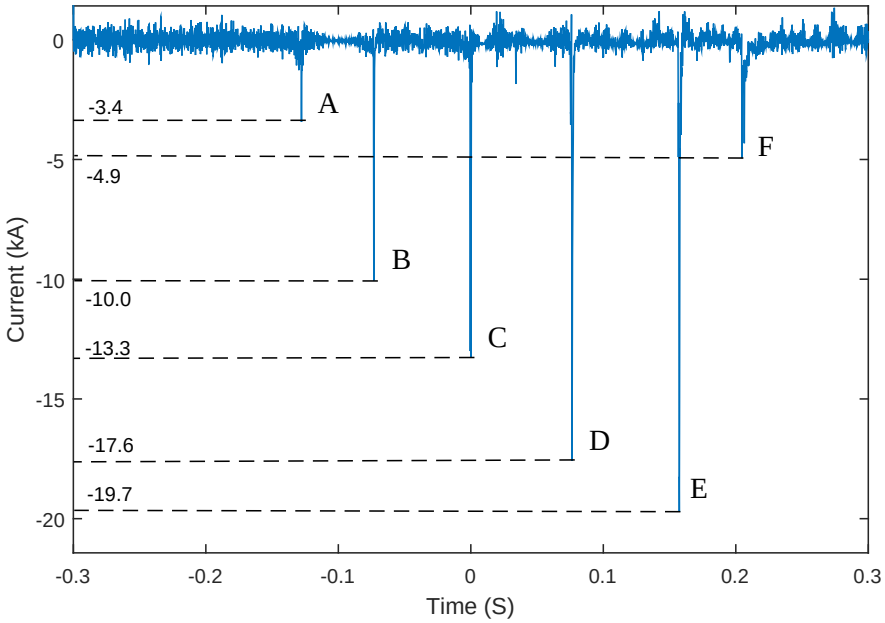

(b)

Figure 4.6: Inferred instantaneous current inferred from electric field recordings with a low pass filter cutoff frequency of 1.5 kHz (4.6(a)) and 2 kHz (4.6(b)).

The lightning stroke demarcated B has increased from -8.9 kA to -10.0 kA (12 %). The lightning stroke, demarcated E, only increased from 19.4 kA to 19.7 kA (1.5 %). If the recording of the two lightning strokes (B and E) have the same frequency spectrum then the change in filter should result in a proportional change to all the lightning events. The non-proportional increase in the peak lightning currents shows that the lightning strokes do no have the same frequency spectrum. It is not possible to determine from this information if the difference in the frequency components of each stroke is a result of the stochastic noise or the actual differences in the lightning strokes. The large noise around the 0 kA level is approximately 1 kA peak.

The filter bandwidth was then increased to 7 kHz and the current for the lightning event inferred again. The current waveform for the lightning event, inferred from the lightning event electric fields with a filter bandwidth of 7 kHz is shown in Figure 4.7(a). The noise around the 0 kA level has a increased significantly as its magnitude is approximately 5 kA. Additionally the peak current of the lightning strokes has increased significantly for all strokes compared to the filter bandwidth of 2 kHz. For example the stroke denoted E has increased from -19.7 kA to -32.8 kA. Furthermore, one of the positive impulses between strokes D and E reaches a peak of 8.0 kA, which is larger in magnitude than strokes A and F for the current inferred with a filter bandwidth of 1.5 kHz.

Lastly a filter bandwidth of 20 kHz was applied to the electric field recording and the lightning current inferred from the electric field data again. The lightning current inferred from the electric field data is shown in Figure 4.7(b). Most notably the noise where no lightning strokes occurred has a magnitude of 20 kA peak. Around stroke A, the actual stroke peak (located at the time of the peak of the current in Figures 4.6(a), 4.6(b) and 4.7(a)) is obscured by a higher magnitude impulse appearing after the time of the stroke. Since the noise in Figure 4.7(b) is larger than strokes A and F, identifying the strokes from the current plot alone is not possible. Additionally the magnitude of the peak current of the lightning strokes has increased significantly. Stroke E, has increased from -32.8 kA to -93.3 kA.

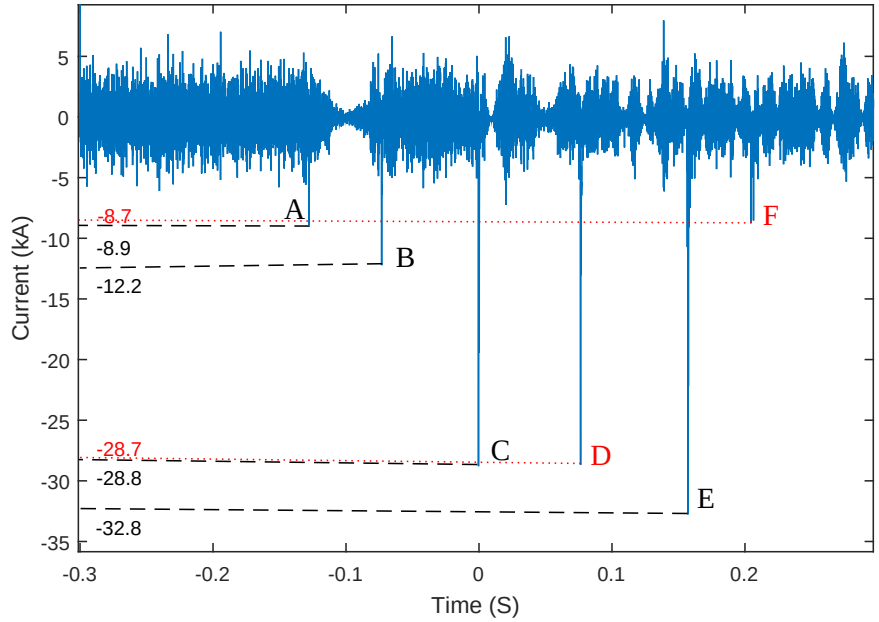

(a)

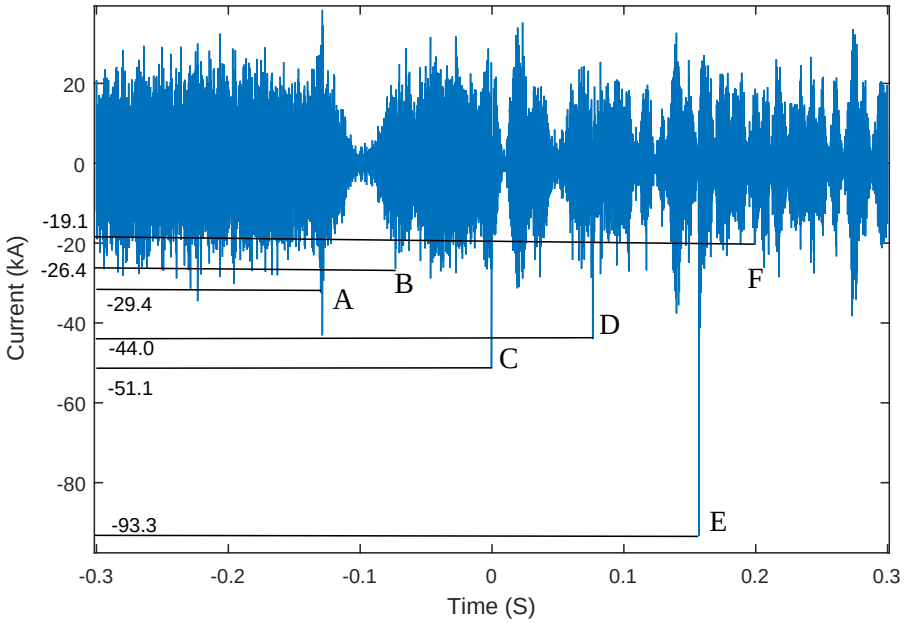

(b)

Figure 4.7: Inferred instantaneous current inferred from electric field recordings with a low pass filter cut-off frequency of 7 kHz (4.7(a)) and 20 kHz (4.7(b)).

Table 4.2: Date and time of lightning strokes recorded by both the South African Lightning detection network and the Electric field sensor. The peak current measured by the Lightning Detection Network (I_{pLDN}) and the electric field sensor (I_{pEF}) is given. The filter bandwidth used was 7 kHz.

Stroke no.	Date and Time	I_{pLDN} (kA)	I_{pEF}(kA)
C	01/03/2015 13:57:13.100	-24.00	-28.8
D	01/03/2015 13:57:13.100	-30.00	-28.7
E	01/03/2015 13:57:13.200	-32.00	-32.8
F	01/03/2015 13:57:13.300	-8.00	-8.7

4.4 Discussion

The lightning current can not be inferred accurately from the lightning electric fields recorded. The relative increases of the lightning strokes compared to the same strokes at a lower bandwidth is not constant. Additionally the magnitude of the noise becomes so large that it is not possible to identify lightning strokes, if the filter bandwidth is too large. The influence of the measurement noise can be attributed to the recorded electric field having a low resolution compared to the relatively large noise magnitude. The signal output from the sensor has a relatively low output signal voltage. Additionally the fast rise time of the electric field for a lightning stroke ($\approx 120\ ms$ for 10% to 90%) means that the bandwidth of the information is approximately 2.5 kHz [26].

It should be noted that there does exist a filter cut-off frequency where the inferred lightning current matches that recorded by the lightning detection network. At a filter bandwidth of 7 kHz the lightning current inferred from the electric fields closely matches that reported by the lightning detection network. Only 4 of the 6 strokes identified from the electric fields was reported by the lightning detection network. The lightning stroke peak current inferred from the electric field data is shown in Figure 4.7(a). The 4 strokes from this event recorded by the lightning detection network is matched to 4 of the 6 strokes observed from the electric fields in Table 4.2. It is noted that the South African Lightning Detection Network has a peak current resolution

of 2 kA.

Analysing Figure 4.5, there does not appear to be a point where the lightning peak current remains constant regardless of the cut-off frequency. In Figure 4.5 around the 7 kHz range the lightning peak current is still changing. This implies that the noise always significantly influences the peak current inferred from the electric field. This means that the magnitude of the signal compared to the noise is too low for accurate analysis. It is noted that the sampling frequency of 1.75 MSps used sufficiently oversampled the signals.

4.5 Possible Solutions

The accuracy of the current inferred from the electric field measurements will be improved if the magnitude of the electric field signal to the noise is increased. The signal can be increased by either making the integrating capacitor smaller (Equation 2.20), or by adding an amplifier to the output of the sensor. The noise can be reduced by using measurement equipment with a higher resolution or with lower measurement noise. By this means the effect of the noise will be mitigated without affecting the information contained in the signal. Micro-controllers or affordable analogue to digital converters with a higher resolution and a sampling frequency of at least 2 MSps may improve the results.

4.6 Summary

The methodology presented in Section 3.4 is applied to the electric fields recorded for a lightning event recorded on the 3^{rd} January 2015 13h57m22. The lightning event was 4.28 km from the sensor. The signal is first filtered by a digital phase-less filter to reduce the noise and improve the resolution. The resistive decay inherent to the measurement equipment is then compensated for. The waveform is finally multiplied by the sensor gain to get the electric fields observed by the sensor. This process is repeated for various filter frequencies. The lightning current is inferred for each filter frequency. The lightning strokes were easily identified in the current waveform with the low filter bandwidth of 1.5 kHz. However at higher filter bandwidths (20 kHz)

the noise obscures some of the lightning strokes. The peak current does not remain constant for any filter cut-off frequency which means that the correct filter frequency cannot be inferred. This implies that the magnitude of the signal compared to the magnitude of the noise is too low. Therefore it is not possible to infer the lightning stroke current from the electric fields recorded. Although it is possible to make observations about the polarity, number, charge transferred and duration of the individual strokes.

Chapter 5

Conclusion

The lightning stroke discharges one of the charge centres in the cloud during a cloud-to-ground lightning event. The discharge of the charge centre results in a change in the electric field radiated by the charge centres. Theoretically it is possible to infer the lightning current waveform, from the changes in the electric field radiated by the charge centres. The electric field derivative needs to be determined in order to infer the current from electric field measurements. High frequency measurement noise will be amplified if the derivative process is applied after the electric fields are recorded.

The electric fields for a lightning event was recorded. The sensor used is a flat plate electric field sensor with a passive integrator. The measurement equipment used is known to have relatively large measurement noise. A low pass filter was applied to the recordings to isolate the lower frequency components of the signal. Multiple filter cut-off frequencies were used to analyse the effects of various frequency components on the electric field measurements. The lightning current was then inferred from the resulting electric fields. The inferred peak lightning current was compared to the lightning stroke current recorded by the South African Lightning Detection Network. At low filter cutoff frequencies (1.5 kHz and 2 kHz) the individual strokes were easily identified. However at higher filter cutoff frequencies (20 kHz) the noise obscured some of the lightning strokes. The peak inferred lightning current did not remain constant for any filter bandwidth. Increases in the

filter bandwidth did not result in consistent increases in the peak stroke currents. This implies that the individual strokes contained different frequency components.

The number of strokes, polarity and charge transferred of the lightning strokes can be inferred from the lightning electric fields recorded. As expected due to the measurement noise, which had a magnitude in the digital recording of 3 to 4 discrete steps, the lightning current cannot be accurately inferred from the electric field waveforms recorded, which had a peak magnitude of 21 discrete steps.

Appendix A

Paper Submitted to ICLP

A.1 Preamble

This appendix is a paper that was accepted and presented for publication in the 32^{nd} *International Conference on Lightning Protection* in October 2014, hosted in Shanghai, China. The paper is titled **Comparison Between Numerical and Passive Integration of Flat Plate Electric Field Sensor Output**

A.2 Paper Description

This paper describes a calibration experiment performed to determine the best configuration for the electric field sensor, for the application of the experiments conducted to obtain the data presented in Chapter 4 and Appendix B. The calibration involved creating a known electric field against which the output of the sensor was compared.

2014 International Conference on Lightning Protection (ICLP), Shanghai, China

Comparison Between Numerical and Passive Integration of Flat Plate Electric Field Sensor Output

J. H. Lange, H.G.P. Hunt, K.J. Nixon
School of Electrical & Information Engineering,
University of the Witwatersrand, Johannesburg,
Private Bag 3, Wits 2050,
Johannesburg, South Africa

***Abstract*—It is required to determine the best configuration for sensors to be used to in an electric field study on lightning occurring in the Johannesburg region. The tests performed were to determine the best sensor configuration to be used and to validate sensor output against a known source. Using a pair of flat plates an impulse was applied to the flat plates resulting in a known electric field. The output of the flat plate electric field sensor, was then compared to the known input. It was shown that despite the resistive load being the simplest to implement, it resulted in problems that require more advanced acquisition tools. Whereas using the passive integration of a capacitor, resulted in a more accurate output, which does not require complex acquisition hardware.**

Keywords—flat plate sensor; calibration; lightning; electric fields

I. INTRODUCTION

A lightning electric field study will be performed within Johannesburg, South Africa. In order to measure the electric fields of the lightning events a flat plate sensor will be used. Calibration is important before field tests are conducted. In order to perform a calibration, a reference field is created by using a large pair of flat plates to create a semi-uniform electric field. The sensor is placed in this field and the output of the sensor is compared to the expected fields created by this field.

A background to lightning physics and the project to measure lightning electric fields in Johannesburg, South Africa is presented, followed by a description and analysis of the sensor. The experimental setup is then described followed by the methodology, the results and some preliminary analysis.

II. BACKGROUND

It is of interest to record the electric field waveforms for naturally triggered cloud to ground lightning in Johannesburg, South Africa. Figure 1 shows the proposed sensor location for the test. This experiment will measure the changes of the charge within a thundercloud. The location is within 2 km of the Sentech Tower at an altitude of 1600 m. Therefore the lightning strokes to be witnessed may attach to the tower. This will be verified using visual evidence from a camera monitoring the tower [1, 2].

In a thundercloud, charges separate to form a tripole arrangement, with a positive charge centre on top, a negative charge in the middle and a smaller positive charge at the bottom. These charges create an electric field between the cloud and the ground. When a lightning stroke moves some of these charges to ground, there is a resultant change in the cloud to ground electric field [3]. This cloud to ground electric field can be measured with a field mill. However the bandwidth limitation of a field mill (DC-1 kHz) does mean that field mills can only provide a limited amount of information. Flat plate electric field sensors have a much higher bandwidth (1 kHz-10 MHz) and can thus capture more information. Flat plate electric field sensors produce a current which is proportional to the incident electric field derivative. By placing various loads upon the output of the sensor, various output forms are available from the sensor [4–7].

Fig. 1. Proposed test location for lightning electric field study, with Sentech tower in the background.

Following the design of a battery powered measurement unit, it is of interest to determine the best configuration of the sensor for these units. As such, characterising the output from the sensor by performing various calibration tests is of importance before the lightning occurs. This means that information from the sensor can be used reliably [8].

978-1-4799-3544-4/14/$31.00 ©2014 IEEE

(a)

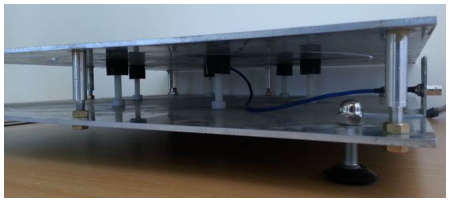

(b)

Fig. 2. Top view (a) and side view (b) of sensor used

III. Flat Plate electric field sensor

The flat plate sensor used in this paper is shown in Figure 2. The design of the flat plate sensor follows that presented by Jerauld [4]. The sensor contains a 0.444 m diameter aluminium disc, called the sensor plate, held flush with the top of the sensor, separated by a 5 mm annular gap. The frame of the sensor, is a square 0.54 m in length. The frame of the sensor is earthed, while the sensor plate is connected to the signal line of a BNC connector. The sensor plate is held isolated with nylon bolts that are topped with plastic caps, used to hold off water. The aluminium of the sensor is 4 mm thick, to help the sensor resist damage from hail. Special attention was paid to keep the top of the sensor as flat as possible and free from protrusions that may lead to electric field concentrations.

A. Basic Output

The charge on a conductor exposed to a field is proportional to the component of the incident field perpendicular to the plates surface. Provided the field is uniform, the charge can be described by Equation 1 [4, 9].

$$Q_{plate} = \epsilon_0 A_{plate} E_{\perp} \tag{1}$$

Where, Q_{plate} is the charge on the plates, A_{plate} is the surface area of the plate, $E_{\perp}$ is the component of the incident electric field perpendicular to the plate surface and ϵ_0 is the permittivity of free space. It can be said that the incident field on the sensor plate is uniform if the field wavelength is much larger than the plate diameter. Generally the maximum frequency of the lightning electric field is assumed to be about 30 MHz which has a wavelength of 10 m [4]. The diameter of the plate of 0.444 m is less than $1/20$ of a wavelength, meaning a uniform incident field can be assumed. From Equation 1 and the definition of current, as given in Equation 2, the Norton short circuit current of the sensor can be determined.

$$i(t) = \frac{d}{dt} Q_{plate}(t) = \epsilon_0 A_{plate} \frac{dE_{\perp}(t)}{dt} \tag{2}$$

Thus the sensor can be modelled as an electric field derivative dependant current source. There is a parasitic capacitive and inductive elements that can be considered, however their effects are largely negligible compared to the loads that are used on the sensor [4].

B. Field Derivative Sensor (Numerical Integration)

The simplest load that is used on the sensor is a resistor. In this configuration the voltage output from the sensor will be a voltage proportional to the field derivative as given in Equation 3 [4].

$$v(t) = R_{load} \epsilon_0 A_{plate} \frac{dE_{\perp}(t)}{dt} \tag{3}$$

Where R_{load} is the load resistance applied to the sensor plate. Usually for matching reasons the resistor used is the same impedance as the surge impedance of the co-axial cable used to connect the cable to the sensor. Once the field derivative data has been captured the samples need to be numerically integrated. This is done using Equation 4 [10].

$$I(n) = D(n) * dt + I(n-1) \tag{4}$$

Where $I(n)$ is the numerical integration for the n^{th} sample $D(n)$ the n^{th} derivative sample and dt is the time between each sample.

C. Field Sensor (Passive Integration)

An alternative load is a capacitor load. The capacitor acts as a passive integrator integrating the current from the sensor as described in Equation 5.

$$v(t) = \frac{1}{C_{int}} \int i(t) dt = \frac{1}{C_{int}} \int \epsilon_0 A_{plate} \frac{dE_{\perp}(t)}{dt} dt \tag{5}$$

Where C_{int} is the capacitance used. The final ideal output of the sensor is thus described by Equation 6.

$$v(t) = \frac{1}{C_{int}} \epsilon_0 A_{plate} E_{\perp} \tag{6}$$

In order to enforce a known decay time upon the integrator a resistor is usually connected in parallel with the capacitor.

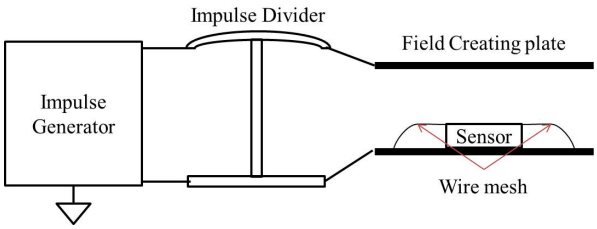

Fig. 3. Experimental setup used for field creation

D. Digital Storage Oscilliscope (DSO)

Lightning events are stochastic and thus making any measurement on a lightning event is challenging, especially if trying to record events that have a signal bandwidth higher than 1 MHz. This is due to the large amount of data that will need to be stored and processed when sampling at high speeds. Modern DSO's utilise analog-to-digital converters to convert analogue voltages into digital data. However the resolution of these recordings is typically 8-bits due to limitations of current technology. This means that significant small signal data can be lost. While this is sufficient for visual inspection, the lack of resolution leads to significant issues for numeric processing. Oscilloscope designers often compensate against the lack of resolution by oversampling a signal at sample rates much higher than required. This does provide additional information, not to numeric analysis, without additional post-processing [10].

IV. Experimental Setup

Figure 3 shows the experimental setup used to apply a field to the sensor. In order to create the semi-uniform electric field, from which the measured signals will be compared, a large flat plate is held electrically isolated above the sensor. Another plate is placed below the sensor to simulate the earth. These plates are 1.80 m in both length and breadth. Wire mesh with a mesh hole diameter of 80 mm is then placed level with the sensor. The wire mesh smooths the interface between the sensor and the air to negate any electric field enhancement that would occur due to the sharp edges of the sensor frame. The field in the gap created between the field creation plates is linearly proportional to the voltage applied to the top plate and can be approximated by Equation 7.

$$E_{gap} = V_{plate}/d \tag{7}$$

Where E_{gap} is the electric field between the top plate and the top of the sensor, V_{plate} is the voltage applied across the field creation plates and d is the distance between the top plate and the top of the sensor. The voltage applied to the field creation plates, shown in Figure 4, is generated from a 5-stage Marx Generator passed through a shaping circuit. The shaping circuit was modified to produce the desired field derivatives and changes expected from previous studies. The rise and fall times of the test setup are $1.58\ \mu s$ (from 10% to 90%) and $205\ \mu s$ (from 90% to 10%). A voltage peak of 80 kV was used for all the tests. The polarity of the voltage used for this experiment was kept positive for all experiments. Coaxial cable (RG-58) with a characteristic impedance of 50Ω connects the sensor to the load and oscilloscope. This cable is shielded by earthed copper pipe.

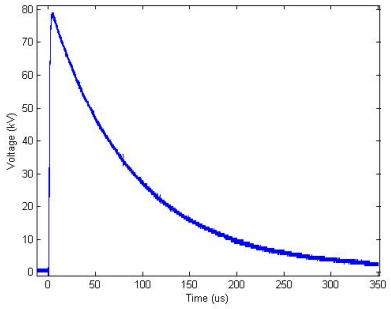

Fig. 4. Example of voltage applied across field creation plates

The loads place upon the sensor were placed within aluminium enclosures to avoid interference. The field derivative sensor is implemented with a $49.9\ \Omega$ surface mounted resistor, the impedance thereof was verified to be $49.82\ \Omega$. Two capacitor loads of 460 nF and 184 nF are used to perform the passive integration for the electric field measurements. These capacitor loads consisted of 100 nF surface mount X7R ceramic capacitors. A frequency sweep was performed on each load box to ensure each load behaved as capacitors for the frequency range of DC-10 MHz. The loads are connected as close as possible to the oscilliscope.

The oscilloscope used for the calibration process is a Rigol DS6062E. This 600 MHz bandwidth and 5 GSa/sec with a 140 Million Sample memory allows for the raw samples to be imported into a standard personal computer for accurate post processing. In order to gain additional information from the oversampled signals, from the oscilloscope, a low pass filter is applied to the samples. Since lightning based measurements are time-based measurements, important characteristics are a wide-bandwidth as well as a negligible phase shift. In order to extract a higher effective resolution from the data, while negating higher frequency components a digital low pass filter is used. Since the frequency components of the waveforms expected from the calibration setup are less than 500 kHz, the filter can be appropriately designed. The filter used is an 8th order low pass filter, using a zero-phase digital filter algorithm, with a -6 dB point of 1 MHz. The results of this post processing is shown in Figure 5 from which it can be seen that there is no phase shift [11].

V. Methodology

For this evaluation four different experiments were carried out. Each experiment implemented a different load, or

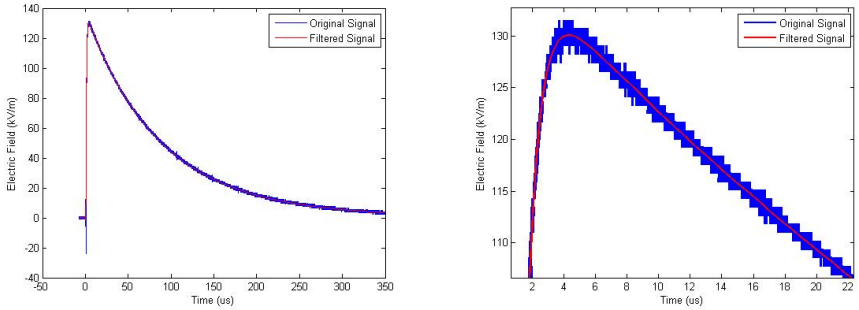

(a) (b)

Fig. 5. Comparison of an original samples and filtered signal of all samples(a) and some samples(b).

measurement technique, however the physical setup, voltage applied and sensor did not change between experiments. For each of these experiments the sample-by-sample error waveform was then obtained, using Equation 8.

$$Err[n] = \frac{E_{gap}[n] - E_{sensor}[n]}{E_{gap}[n]} \tag{8}$$

- A1: Field Derivative sensor. A 50 Ω load was connected to the sensor, and an impulse applied to the field creation plates. The oscilliscope was adjusted so as to avoid any clipping of the waveform. The waveforms of the voltage applied to the field creation plates, as well as the output from the sensor were then scaled by the appropriate gains, presented in Equations 3 and 7 to obtain the waveforms in terms of the electric fields. A numerical integration was then performed upon the derivative signal.
- A2: Field Derivative sensor, with oscilliscope clipping. Clipping refers to the oscilliscope being unable to record certain signals as the magnitude is outside the measureable range of the oscilliscope for a particular voltage scale. A 50 Ω load was connected to the sensor, and the oscilliscope's voltage scale was reduced, to allow initial clipping but to acquire more resolution of smaller signals. An impulse was applied to the field creation plates. The waveforms were then scaled appropriately, according to Equations 3 and 7 and the output from the sensor was numerically integrated.
- B1: Field Sensor with 460 nF load. The 460 nF load was connected to the sensor and an impulse applied. The waveform from the sensor was then post-processed by applying a discrete low pass filter before being scaled appropriately using equations 6 and 7.
- B2: Field Sensor with 184 nF load. The 184 nF load was connected to the sensor and an impulse applied. The waveform from the sensor was then post-processed by applying a discrete low pass filter before being scaled appropriately using equations 6 and 7.

VI. Results

For these results a reference graph has been included in the figures. This waveform is a normalised representation of the voltage applied to the field creation plates over time.

A. Field derivative sensor.

The output waveforms for A1, are presented in Figure 6. It was noted in the raw sensor output, located in Figure 6(a) that the large differences in the output during the rise and fall times of the raw signal resulted in errors. The difference is due to the lower sensor output from the tail due to the lower derivative compared to the shorter rise time. Either a loss of resolution of the fall time or clipping of the rise time was unavoidable with the limited resolution of the scope. The resolution was improved for the tail of the waveform by reducing the voltage scale of the oscilloscope to focus on the tail time of the waveforms, resulting in clipping of the measurement during the rise time (A2). The resultant electric fields from this change in focus are shown in Figure 7.

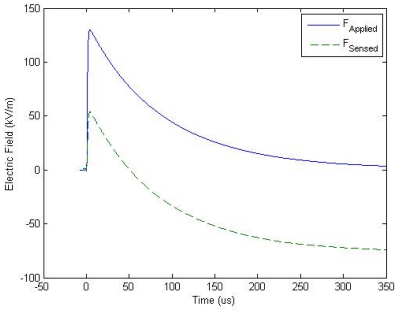

Fig. 7. Numerically integrated field output vs time for Experiment A2.

Due to the clipping that occurs when the oscilloscope is zoomed into the tail of the waveform, information about the rise time and hence the peak of the waveform is lost.

B. Electric field sensor

Using the two different capacitive loads, the waveform for each load is presented in Figure 8. The individual samples

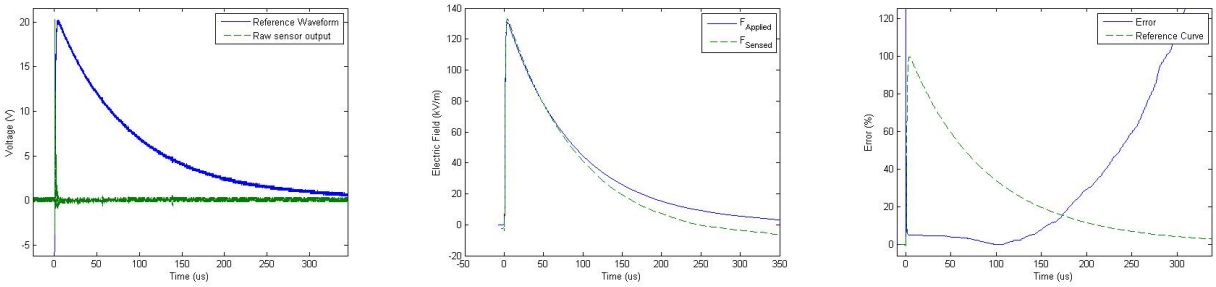

(a) (b) (c)

Fig. 6. Results from Experiment A1, showing sensor output vs. time (a), integrated sensor output vs. time (b) and sample, by sample error vs time (c)

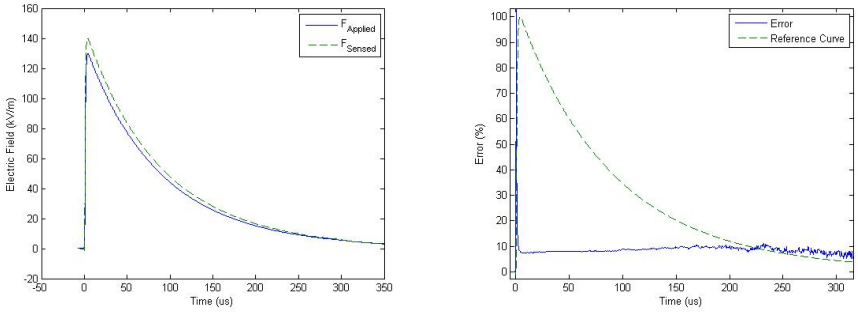

(a) (b)

Fig. 8. Results from experiment B1 showing the sensor output vs. time (a) and the sample by sample error vs. time (b)

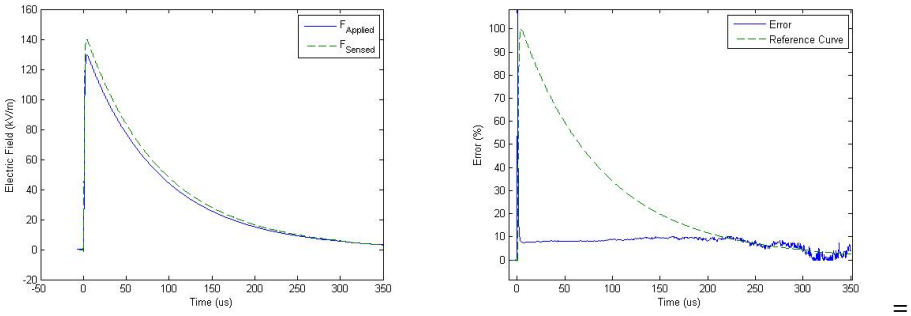

(a) (b)

Fig. 9. Results from experiment B2 showing the sensor output vs. time (a) and the sample by sample error vs. time (b)

were compared to each other to produce the error waveforms shown in Figure 9.

VII. Discussion

A. Field Derivative

The use of a resistor to load the sensor is advantageous where a transmission line is required to get the signal from the sensor some distance to the recording instruments. This technique often involves the use of a matched resistive load, to the transmission line, reducing the issues of mismatching. However the use of this load produces signals with higher bandwidths, thus requiring acquisition systems with a high sampling frequency and consequently a large sample memory. This results in a few issues. As lightning fields have various high and low frequency components, the higher frequency components may saturate the measurement while the lower frequency components are barely noticeable due to the derivative action of the sensor. When integrating the samples obtained with this method, the lower frequency components may be lost by the lack of resolution if the higher frequency components are of primary interest. This may result in no errors on a

rise time, but large errors on the fall time. A solution to this problem is to use multiple channels on the acquisition unit, with various gains. This will allow for the accurate capture of the large signal components that make up the rise times, while still retaining a higher degree of accuracy of the lower frequency components. This requires more complex equipment, which may not be feasible.

B. Field Sensor

Using a capacitive passive integrator has the advantages of reducing the bandwidth of the output signal, as well as performing the integration more accurately for the entire waveform. It does however produce matching errors should any form of transmission line be used to connect the sensor to the load. Furthermore the results are dependent on an accurate measurement of capacitance, which is often difficult to measure accurately. This load is well suited to battery powered measurement systems, as the lower bandwidth of the output signal allows for lower sampling rates. Additionally should the measurement system and the passive integrators be placed as close as possible to the sensor then the mismatch issues should be largely negated. It is noted that the errors for both capacitive loads were constant at approximately $10\ \%$. This indicates an error in the test setup, possible attributable to an error in the voltage multiplier or some minor field enhancement. The use of operational amplifiers to construct an active integrator is a solution that may also need to be investigated for its accuracy and feasibility.

VIII. Conclusion

An experimental setup to create a semi-uniform field was used to calibrate a flat plate electric field sensor that is to be used to measure the electric fields of a lightning strike. A series of impulses was applied to the field creating plate and the sensor output was compared to the voltage applied to field. Although the field derivative setup was the simplest and does not produce any mismatch errors, the numerical integration process required resulted in errors in output from the field derivative setup. Furthermore the field derivative output has a higher bandwidth than the input field output. The passive integration setup resulted in a lower bandwidth. Additionally the error using the passive integrator setup is a constant error, which is more attributable to an error in the gain constants. The downside to using the passive integrator is that the measurement system needs to be as close as possible to the sensor to negate mismatch errors. Since the electric field experiment to be conducted will utilise a high resolution, low frequency measurement system, it is more appropriate to make use of the electric field sensor, using the passive integrator technique.

ACKNOWLEDGMENTS

The authors would like to thank CBI-electric for funding the Chair of Lightning at the University of the Witwatersrand and for direct support of the Research Group. They would also like to thank Eskom for the support of the Lightning/EMC Research Group through the TESP programme. Thanks are extended to the department of Trade and Industry (DTI) for THRIP funding as well as to the National Research Foundation (NRF) for direct funding of the Research Group.

References

[1] R. A. Serway and J. W. Jewett. *Comparison between South African lightning detection network interpretation of single-channel and branched upward lightning flashes to a tall structure*. Brooks Cole, 7th editio ed., Oct. 2007. URL http://ieeexplore.ieee.org/lpdocs/epic03/wrapper.htm?arnumber=6729232.

[2] Y. Liu, H. Hunt, M. D. Grant, and K. Nixon. "Observations of Lightning Discharges on Brixton Tower." In *30th International Conference on Lightning Protection - ICLP 2010*, vol. 2010, p. 1504. Cagliari, Italy: Brooks Cole, 2007.

[3] M. A. Uman. *The Lightning Discharge*. Courier Dover Publications, 2001.

[4] J. E. Jerauld. *Properties of Natural Cloud-to-Ground Lightning Inferred from a Multiple-Station Measurements of Close Electric and Magnetic Fields and Field Derivatives*. Ph.D. thesis, University of Florida, 2007.

[5] M. A. Haddad, V. A. Rakov, and S. A. Cummer. "New measurements of lightning electric fields in Florida: Waveform characteristics, interaction with the ionosphere, and peak current estimates." *Journal of Geophysical Research*, vol. 117, no. D10, p. D10101, May 2012. URL http://doi.wiley.com/10.1029/2011JD017196.

[6] M. Mohanty and P. P. Kumar. "Electric field measurements of overhead thunderstorm at a tropical station using network of plate antennas." *Indian Journal of Radio and Space Physics*, vol. 33, no. October, pp. 310–315, 2004.

[7] W. Ibrahim, M. Ghazali, and S. Ghani. "Measurement of Vertical Electric Fields from Lightning Flashes using Parallel Plate Antenna." *International Conference on Electrical, Control and Computer Engineering 2011 (InECCE)*, pp. 466–471, Jun. 2011.

[8] J. Lange, H. Hunt, and K. Nixon. "Design , Testing and Implementation of a Data Acquisition System for Lightning Electric Field Measurements." In *South African Universities Power Engineering Conference 2014*. 2014.

[9] R. A. Serway and J. W. Jewett. *Physics for Scientists and Engineers with Modern Physics*. Brooks Cole, 7th editio ed., 2007.

[10] J. P. Bentley. *Principles of Measurement Systems*. Pearson Education, 2005.

[11] S. W. Smith. "Chapter 19: Recursive Filters." In *The Scientist and Engineer's Guide to Digital Signal Processing*, p. 626. California Technical Publishing, 1997.

Appendix B

Validation experiment

Since it has already been established that the sensor used is an accurate technique of measuring fast electric fields (Appendix A) it is desirable to ensure that the electric fields measured by one sensor system are not influenced by any nearby obstacles or otherwise. In order to establish confidence in the readings an experiment was conducted whereby the experimental setup was replicated to create a second independent measurement system. The measured recordings could be compared from two independent sources, thus establishing that the recordings made of lightning events are the electric fields radiated during a lightning event.

B.1 Overview

Two electric field sensors are placed 5 m apart and connected to independent measurement systems. The two sensors are used to measure the same electric fields from the same lightning event. The resultant electric fields from each system are compared to each other.

B.2 Electric Field Recorded

The vertical electric fields from a lightning stroke occurring on the 26^{th} of November 2014 at 23h20, were recorded by two separate sensors connected to two separate loads on two different oscilloscopes. Sensor A was connected to the 200 nF load, connected to the Rigol DS1102E, whereas Sensor B was

connected to the 500 nF Load connected to the Rigol DS1052E. This results in two independent readings that are processed individually. During this lightning storm there was no rain, so the effects of charged rain on the sensor can be neglected. Due to the independent oscilloscopes triggering slightly differently the time axis of the one recording was adjusted by 4.64 ms in order to align the most significant impulse. The individual electric fields are shown in Figures B.1(a) and B.1(b).

B.3 Analysis

The two waveforms presented in Figure B.1 both present the same artefacts and magnitudes, within a difference in magnitude of approximately 2.5 $kV/m(\approx 10\%)$. Compensating for the initial DC voltage offset by removing the average voltage of the entire set of samples from both sets of samples gives the plot shown in Figure B.2.

It should be noted that the resultant gain of the sensor connected to the 500 nF load is smaller than that connected to the 200 nF load. This means that the voltage recorded by the sensor connected to the 500 nF load is smaller than that connected to the 200 nF load. As a result the signal from the oscilloscope is more prone to errors occurring due to the decreasing resolutions of the oscilloscope for low voltage signals.

However the output from both sensors during the first impulse, as shown in Figure B.3, are very similar and differ from each other by only 8 % at the peak. However as time progresses, the lower signal from the 500 nF sensor results in increasing errors due to the lack of resolution, leading to what appears to be discrete steps in the plot as shown in Figure B.4.

B.4 Summary

Two independent sensors were placed a small distance apart. Two waveforms were measured for a single lightning event. Although the electric fields from the two sensors do differ significantly as time progresses, the output from the two independent systems is very similar. The largest difference measured is less than 10 % of the full scale reading. Both recordings share similar artefacts and with the exception of certain impulses are exactly the same.

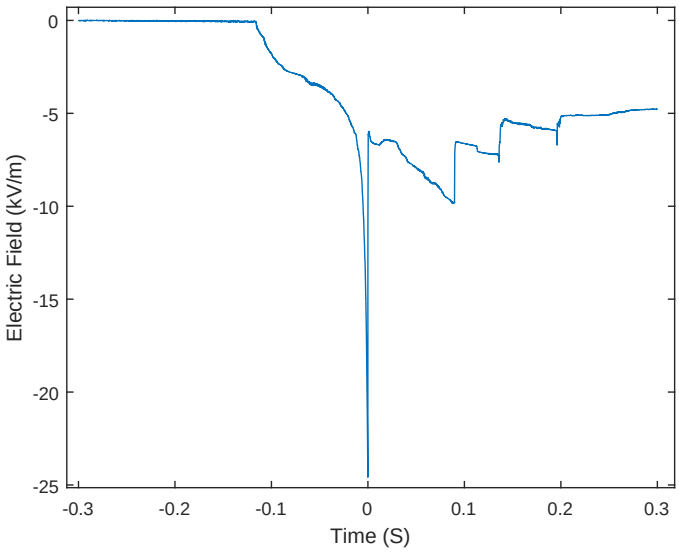

(a)

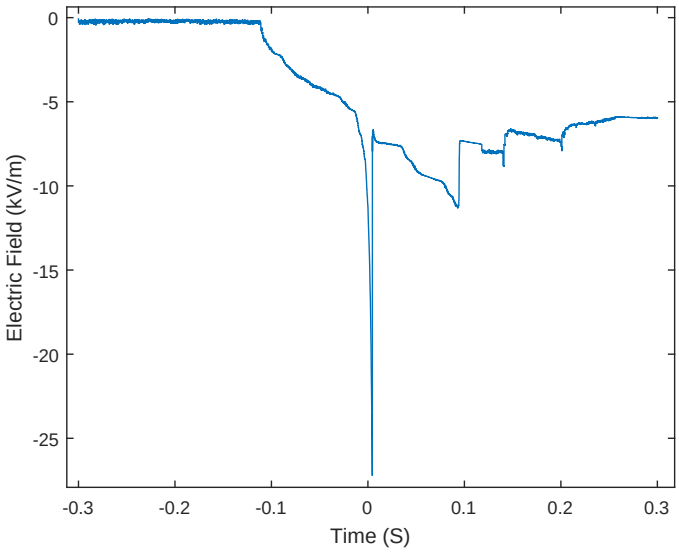

(b)

Figure B.1: Electric field recordings for lightning event occurring 26/11/2014 23h20. Figure B.1(a) was obtained using sensor A, with a 200 nF load. Figure B.1(b) was obtained using sensor B, with a 500 nF load

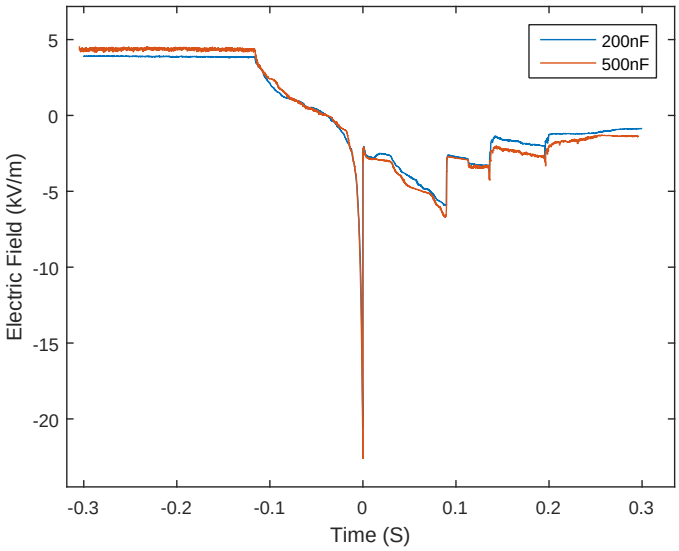

Figure B.2: Electric field recordings for lightning event occurring 26/11/2014 23h20. Both Waveforms have been DC adjusted to have a mean of 0 V/m.

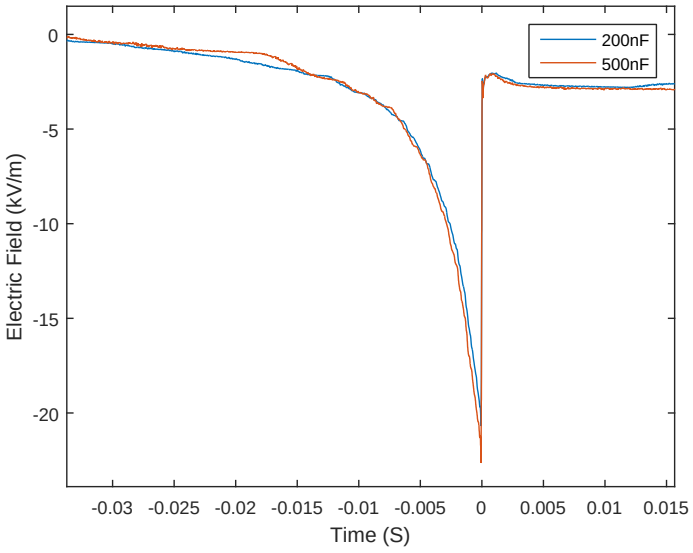

Figure B.3: First impulse in electric field recordings for lightning event occurring 26/11/2014 23h20. Both Waveforms have been DC adjusted to have a mean of 0 V/m.

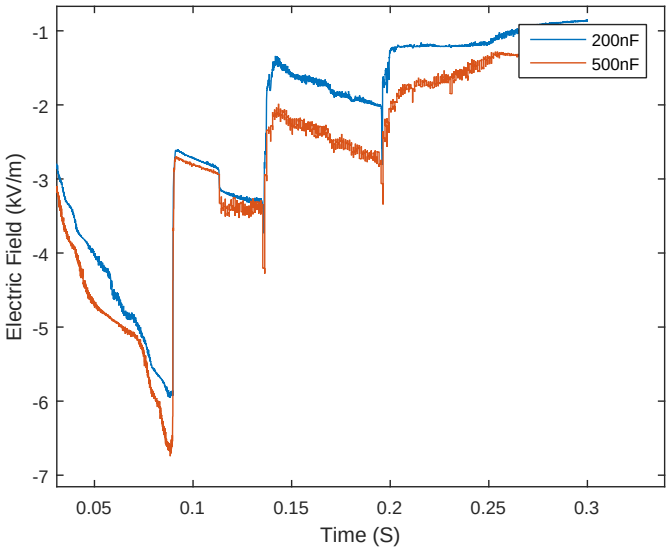

Figure B.4: Remaining impulses in electric field recordings for lightning event occurring 26/11/2014 23h20. Both Waveforms have been DC adjusted to have a mean of 0 V/m.

The test setup and the electric field data obtained can be confidently used.

References

[1] SAPA. "Lightning kills hundreds every year in South Africa.", 2013. URL http://www.timeslive.co.za/local/2013/02/13/lightning-kills-hundreds-every-year-in-south-africa.

[2] I. R. Jandrell, R. Blumenthal, R. B. Anderson, and E. Trengove. "Recent lightning research in South Africa with a special focus on keraunopathology." In *16th International Symposium on High Voltage Engineering*, p. 6. 2009.

[3] E. Trengove and I. R. Jandrell. "Strategies for understanding lightning myths and beliefs." *Lightning Protection (ICLP), 2010 International Conference on*, vol. 7, no. June, pp. 3–8, 2010.

[4] A. C. Britten and A. A. Burger. "Susceptibility of 400kV transmission lines to bird streamers and bush fires." *energize*, , no. December, pp. 25–28, 2011.

[5] M. A. Haddad, V. A. Rakov, and S. A. Cummer. "New measurements of lightning Electric Fields in Florida: waveform characteristics, interaction with the ionosphere, and peak current estimates." *Journal of Geophysical Research*, vol. 117, no. D10, p. D10101, May 2012. URL http://doi.wiley.com/10.1029/2011JD017196.

[6] L. Z. S. Campos, M. M. F. Saba, C. Schumann, and W. Schulz. "Characterization of M components in positive lightning from high-speed video and Electric Field Data." In *3rd International Symposium on Winter Lightning*, pp. 63–66. 2011.

[7] M. Mohanty and P. P. Kumar. "Electric field measurements of overhead thunderstorm at a tropical station using network of plate antennas." *Indian Journal of Radio and Space Physics*, vol. 33, no. October, pp. 310–315, 2004.

[8] H. Zhou, G. Diendorfer, R. Thottappillil, H. Pichler, and M. Mair. "Measured current and close electric field changes associated with the initiation of upward lightning from a tall tower." *Journal of Geophysical Research*, vol. 117, no. D8, p. D08102, Apr. 2012. URL `http://doi.wiley.com/10.1029/2011JD017269`.

[9] T. Gill. "A lightning climatology of South Africa for the first two years of operation of the South African Lightning Detection Network: 2006-2007." In *2nd International Lightning Meteorology Conference*, pp. 1–12. 2008. URL `http://www.vaisala.com/files/A_lightning_climatology_of_South_Africa.pdf`.

[10] C. B. Moore, B. Vonnegut, and D. N. Holden. "Anomalous electric fields associated with clouds growing over a source of negative space charge." *Journal of Geophysical Research: Atmospheres*, vol. 94, no. D11, pp. 13127–13134, 1989.

[11] E. Kuffel, W. S. Zaengl, and J. Kuffel. *High Voltage Engineering Fundamentals*. Butterworth-Heinemann, 2000.

[12] J. E. Jerauld. *Properties of natural cloud-to-ground lightning inferred from a Multiple-Station measurements of close electric and magnetic fields and field derivatives*. Ph.D. thesis, University of Florida, 2007.

[13] N. R. C. Geophysics Study Committee, Geophysics Research Forum, Commission on Physical Sciences, Mathematics and Resources. *The Earth's electrical environment*. Washington, DC: The National Academies Press, 1986. URL `http://www.nap.edu/catalog/898/the-earths-electrical-environment`.

[14] V. A. Rakov and M. A. Uman. *Lightning: Physics and Effects*. Cambridge University Press, 2003.

[15] D. M. Mach and W. D. Rust. "Photoelectric return-stroke velocity and peak current estimates in natural and triggered lightning." *Journal of Geophysical Research: Atmospheres*, vol. 94, no. D11, pp. 13273–13283, 1989.

[16] V. Mazur and L. H. Ruhnke. "Determining the striking distance of lightning through its relationship to leader potential." *Journal of Geophysical Research: Atmospheres*, vol. 108, no. D14, pp. 2156–2202, 2003. URL `http://onlinelibrary.wiley.com/doi/10.1029/2002JD003047/epdf`.

[17] R. A. Serway and J. W. Jewett. *Physics for Scientists and Engineers with Modern Physics*. Brooks Cole, 7th editio ed., 2007.

[18] D. K. Cheng. *Field and Wave Electromagnetics*. Addison Wesley, second edi ed., 1989.

[19] S.-b. Liao, P. Dourmashkin, and J. W. Belcher. "Fields - Chapter 2 Coulomb s Law." In *Physics 8.02 Electricity and Magnetism course notes*, pp. 1–44. MIT, 2004.

[20] P. R. Krehbiel, M. Brook, and R. A. McCrory. "An analysis of the charge structure of lightning discharges to ground." *Journal of Geophysical Research: Oceans*, vol. 84, no. C5, pp. 2432–2456, 1979.

[21] C. Schumann and M. M. F. Saba. "Continuing current intensity in positive ground flashes." Tech. Rep. 1992, INPE - Brazilian National Institue for Space Research: Electricity Atmospheric Group, Brazil, 2012.

[22] J. H. Lange, H. G. P. Hunt, and K. J. Nixon. "Comparison between numerical and passive integration of flat plate electric field sensor output." *2014 International Conference on Lightning Protection (ICLP)*, pp. 746–751, Oct. 2014. URL `http://ieeexplore.ieee.org/lpdocs/epic03/wrapper.htm?arnumber=6973222`.

[23] Rigol Technologies Inc. "Data sheet - DS1000E, DS1000D series digital oscilliscopes.", 2008.

[24] R. Mancini. *Op-Amps for Everyone - Design Reference*. August. Texas Instruments, 2002.

[25] Silicon Labs. "Improving ADC Resolution by oversampling and averaging - AN 118." Tech. rep., Silicon Labs, Austin, Texas, 2013.

[26] B. P. Lathi. *Signal Processing and Linear Systems*. Oxford University Press, internatio ed., 2010.

[27] A. Arrants, B. Brannon, and R. Reeder. "AN-835 application note.", 2015.

[28] Y. Liu, H. Hunt, M. D. Grant, and K. Nixon. "Observations of lightning discharges on Brixton Tower." In *30th International Conference on Lightning Protection - ICLP 2010*, vol. 2010, p. 1504. Cagliari, Italy: Brooks Cole, 2007.

[29] J. Lange, H. Hunt, and K. Nixon. "Design , testing and implementation of a data acquisition system for lightning electric field measurements." In *South African Universities Power Engineering Conference 2014*. 2014.

[30] R. Evert and G. Schulze. "Impact of a new lightning detection and location system in South Africa." In *Inaugural IEEE PES 2005 Conference and Exposition in Africa*, July, pp. 11–15. 2005. URL `http://ieeexplore.ieee.org/xpls/abs_all.jsp?arnumber=1611845`.

[31] H. G. P. Hunt, K. J. Nixon, and I. R. Jandrell. *Comparison between South African lightning detection network interpretation of single-channel and branched upward lightning flashes to a tall structure*. Brooks Cole, 7th editio ed., Oct. 2007. URL `http://ieeexplore.ieee.org/lpdocs/epic03/wrapper.htm?arnumber=6729232`.

[32] H. Hunt, K. Nixon, and I. Jandrell. "Can LDN data provide corroborating evidence for a lightning event at a specific geographic location?" *2012 International Conference on Lightning Protection (ICLP)*, pp. 1–6, Sep. 2012. URL `http://ieeexplore.ieee.org/lpdocs/epic03/wrapper.htm?arnumber=6344405`.

[33] R. W. Sinnott. "Virtues of the Haversine." *Sky and Telescope*, vol. 68, no. 2, p. 159, 1984.

[34] S. H. Ngqungqa. "A critical evaluation and analysis of methods of determining the number of times that lightning will strike a structure." Tech. rep., University of the Witswatersrand, Johannesburg, 2005.

[35] J. E. Jerauld. *A Multiple-Station Experiment to Examine the Close Electromagnetic Environment of Natural and Triggered Lightning*. M.s. thesis, University of Florida, 2003.

[36] E. M. Thomson. "A theoretical study of electrostatic field wave shapes from lightning leaders." *Journal of Geophysical Research: Atmospheres*, vol. 90, no. D5, pp. 8125–8135, 1985.

[37] H. Bekker. *An in-depth study into the various factors contributing to the unexplained Line Faults on a large High Voltage network.*. Ph.D. thesis, University of Natal, 2003.

[38] X. Meng, B. H. Zhou, B. Yang, and K. E. Zhu. "Analysis on influence of tall tower on lightning current measurement." *2012 6th Asia-Pacific Conference on Environmental Electromagnetics (CEEM)*, pp. 145–147, Nov. 2012. URL `http://ieeexplore.ieee.org/lpdocs/epic03/wrapper.htm?arnumber=6410587`.

[39] F. Breu, S. Guggenbichler, and J. Wollmann. "Broadband and HF radiation from cloud flashes and narrow bipolar pulses." *Vasa*, 2008. URL `http://medcontent.metapress.com/index/A65RM03P4874243N.pdf`.

[40] J. Chubb. "Chapter 3. Measuring instruments." In *An Introduction to Electrostatic Measurements*, pp. 12–44. John Chubb Instrumentation Ltd, 2009.

[41] J. Chubb. "Chapter 4. Practical electrostatic measurements." In *An Introduction to Electrostatic Measurements*, pp. 45–63. John Chubb Instrumentation Ltd, 2009.

[42] J. R. Lucas. "Chapter 9. High voltage testing." In *High Voltage Engineering*, p. 18. Department of Electrical Engineering, University of Moratuwa, Sri Lanka, 2001. URL `http://www.elect.mrt.ac.lk/HV_Chap9.pdf`.

[43] U. Minnar. "Characterisation of power system events on South African transmission power lines." *Electric Power Systems Research*, vol. 88, no. July 2012, pp. 25–32, 2012.

[44] V. Bourscheidt, O. J. Pinto, K. P. Naccarato, and I. R. Pinto. "Ded-pendance of CG lightning density on altitude, soil type and land surface tempreture in South of Brazil." In *20th International Lightning Detection Conference*, Semc 2002, p. 5. 2008.

[45] J. L. Crissinger. "Design and construction vs. weather." *Interface*, 2005.

[46] M. D. Grant. *Design of a re-usable rocket for triggered-lightning experiments*. Ph.D. thesis, University of the Witwatersrand, 2006.

[47] J. Lange, H. Hunt, and K. Nixon. "Design, testing and implementation of a data aquisition system for lightning electric field measurements." *South African Universities Power Engineering Conference 2014*, 2014.

[48] L. Z. S. Campos, M. M. F. Saba, T. A. Warner, E. P. Krider, K. L. Cummins, and R. E. Orville. "Does the average downward speed of a lightning leader change as it approaches the ground? An observational approach." In *21st International Lightning Detection Conference*, pp. 1–12. 2007.

[49] J. Jerauld, M. Uman, V. . Rakov, K. J. Rambo, and G. H. Schnetzer. "Electric and magnetic fields and field derivatives from lightning stepped leaders and first return strokes measured at distances from 100 to 1000 m." *Journal of Geophysical Research: Atmospheres*, vol. 113, no. 17, pp. 1–15, 2008.

[50] J. E. Dye, M. G. Bateman, H. J. Christian, E. Defer, C. a. Grainger, W. D. Hall, E. P. Krider, S. a. Lewis, D. M. Mach, F. J. Merceret,

J. C. Willett, and P. T. Willis. "Electric fields, cloud microphysics, and reflectivity in anvils of Florida thunderstorms." *Journal of Geophysical Research: Atmospheres*, vol. 112, no. 11, pp. 1–18, 2007.

[51] J. Mäkelä. "Electromagnetic Signatures of lightning near the HF frequency band.", 2010.

[52] M. Izadi, M. Z. A. Ab Kadir, C. Gomes, and V. Cooray. "Evaluation of lightning return stroke current using measured Electromagnetic Fields." *Progress in Electromagnetics Research*, vol. 130, pp. 581–600, 2012.

[53] K. H. Carpenter. "Field of a finite line charge." In *EECE557 Course Notes*, pp. 3–4. Kansas State University, 2008.

[54] E. D. C. Ferraz, M. M. F. Saba, and O. P. Jr. "First measurments of continuing current intensity in Brazil." In *X International Symposium on Lightning Protection*, pp. 189–191. 2009.

[55] A. Nag, V. A. Rakov, W. Schulz, M. M. F. Saba, R. Thottappillil, C. J. Biagi, A. O. Filho, A. Kafri, N. Theethayi, and T. Gotschl. "First versus subsequent return-stroke current and field peaks in negative cloud-to-ground lightning discharges." *Journal of Geophysical Research: Atmospheres*, vol. 113, no. 19, 2008.

[56] Naidu & Kamaraju. *High Voltage Engineering*. McGraw-Hill, 4th editio ed., 2009.

[57] J. P. Nelson. "High-altitude considerations of electrical power systems and components." *IEEE Transactions on Industry Applications*, vol. 1A-20, no. 3, pp. 407–412, 1984.

[58] J. Rai, D. K. Sharma, R. Chand, K. Kumar, and M. Israil. "Horizontally and vertically polarized components of lightning electric fields." In *19th International Lightning Detection Conference*, pp. 1–8. Tucson Arizona, USA, 2006.

[59] I. R. Pinto, O. J. Pinto, D. R. de Campos, and K. P. Naccarato. "Large peak current cloud-to-ground lightning flashes in Southeastern Brazil." *20th International Lightning Detection Conference*, 2006.

[60] A. Barwise. "Lightning and Surge Protection for PV systems on Solar Panel." *Electricity and Contol, Crown Publications*, pp. 41–42, Oct. 2013.

[61] M. Marzinotto, G. Mazzanti, C. Mazzetti, and V. Galbani. "Lightning and switching impulse levels selection for long DC cable lines." *Electrical Insulation and Dielectric Phenomena (CEIDP), 2011 Annual Report Conference on*, vol. 1, no. 1, pp. 510–513, 2011.

[62] W. Schulz and G. Diendorfer. "Lightning characteristics as a function of altitude evaluated from Lightning Location Network Data." *International Conference on Lightning and Static Electricity*, pp. 1–5, Jun. 1999. URL `http://www.sae.org/technical/papers/1999-01-2310`.

[63] L. Peter and F. Mokhonoana. "Lightning detection improvement FALLS brought to Eskom's transmission line design and fault analysis." In *21st International Lightning Detection Conference*, p. 6. Midrand, South Africa: Eskom - Trans Africa Projects, 2010.

[64] J. C. Willett and D. M. LeVine. "Lightning return-stroke current waveforms aloft, from measured field change, current and channel geometry." *Journal of Geophysical Research: Atmospheres*, vol. 113, no. D7, p. 28, 2002.

[65] B. P. Lathi. *Linear Systems and Signals*. Oxford University Press, 2009.

[66] M. M. F. Saba, W. Schulz, and L. Z. S. Campos. "M components or cloud-to-ground subsequent strokes?" In *21st International Lightning Detection Conference*, p. 9. 2010.

[67] W. Ibrahim, M. Ghazali, and S. Ghani. "Measurement of vertical electric fields from lightning flashes using parallel plate antenna." *International*

Conference on Electrical, Control and Computer Engineering 2011 (InECCE), pp. 466–471, Jun. 2011.

[68] R. Malewski, R. P. Corcoran, K. Feser, T. McComb, C. Nellis, and G. Nourse. "Measurements of the transient electric and magnetic field components in HV laboratories." *IEEE Transactions on Power Apparatus and Systems*, vol. PAS-101, no. 12, pp. 4452–4459, 1982.

[69] N. D. Murray, E. P. Krider, and J. C. Willett. "Multiple pulses in dE / dt and the fine-structure of E during the onset of first return strokes in cloud-to-ocean lightning.", 2004.

[70] National Meteorological Library and Archive. "National Meteorological Library and Archive Fact sheet 2 Thunderstorms.", 2011.

[71] R. Thottappillil and V. A. Rakov. "On different approaches to calculating lightning electric fields." *Journal of Geophysical Research: Atmospheres*, vol. 106, no. D13, pp. 14191–14205, 2001.

[72] A. Smorgonskiy, F. Rachidi, M. Rubinstein, and G. Diendorfer. "On the relation between lightning Flash density and terrain elevation." *2013 International Symposium on Lightning Protection*, pp. 62–66, Oct. 2013. URL `http://ieeexplore.ieee.org/lpdocs/epic03/wrapper.htm?arnumber=6729216`.

[73] D. R. Poelman. *On the Science of Lightning : An Overview*. Royal Meteorological Institute of Belgium, 2010.

[74] K. Burger, R. B. Anderson, and H. Kroninger. "Parameters of lightning flashes." *Electra*, vol. 80, pp. 23–37, 1975.

[75] W. Smith. *Principles of ozone generation*. Watertec Engineering, 2008.

[76] W. Shi and Q. Li. "Research on the charge distribution of lightning stepped leader considering the branches." In *2014 International Conference on Lightning Protection (ICLP)*, 2, pp. 1361–1364. Ieee, Oct. 2014. URL `http://ieeexplore.ieee.org/lpdocs/epic03/wrapper.htm?arnumber=6973342`.

[77] M. A. Uman. *The Lightning Discharge*. Courier Dover Publications, 2001.

[78] M. Gijben. "The South African Weather Service lightning climatology." *Watt Now*, Apr. 2012. URL `http://www.wattnow.co.za/article.php?id=732`.

[79] M. Wu, Dong, Li, Ming, Kvarngren. "Uncertainties in the application of atmospheric and altitude corrections as recommended in IEC standards." *16th International Symposium on High Voltage Engineering*, vol. 1, no. 1, pp. 3–8, 2009.